Canadian Geotechnical Journal
Revue canadienne de géotechnique

# Modelling the post-failure stage of rainfall-induced landslides of the flow-type



| | |
|---|---|
| Journal: | *Canadian Geotechnical Journal* |
| Manuscript ID: | cgj-2012-0375.R1 |
| Manuscript Type: | Article |
| Date Submitted by the Author: | n/a |
| Complete List of Authors: | Cascini, Leonardo; University of Salerno, Dept. Civil Engineering<br>Cuomo, Sabatino; University of Salerno, Dept. Civil Engineering<br>Pastor, Manuel; Universidad Politecnica de Madrid, Department of Applied Mathematics and Computer Science<br>Sacco, Claudia; University of Salerno, Dept. Civil Engineering |
| Keyword: | landslide, flow, failure, post-failure, modelling |
| | |

# Modelling the post-failure stage of rainfall-induced landslides of the flow-type

Cascini L. [(1)], Cuomo S. [(1)], Pastor M. [(2)], Sacco C. [(1)]

**Abstract**

The geomechanical modeling of failure and post-failure stages of rainfall-induced shallow landslides represents a fundamental issue to properly assess the failure conditions and recognize the potential for long travel distances of the failed soil masses.

Considering that these phenomena are among the most catastrophic natural hazard, as a contribution to the topic, the paper discusses the potentialities of a hydro-mechanical coupled FEM model to analyze the post-failure stage using an advanced constitutive model. Particularly, simple undrained triaxial tests and experimental evidences of centrifuge tests are reproduced firstly, for both cases of loose and dense soils. Then, two slope scale benchmarks are analyzed in the cases of vertical downward or horizontal water seepage and for both loose and dense soils. Compared with results obtained through standard limit equilibrium analyses, coupled FEM model provides a new comprehensive framework for failure and post-failure scenarios which includes a significant reduction of mean effective stresses also in the case of a loose soil slope subjected to vertical downward water seepage.

The obtained results are particularly encouraging since they outline the possibility to analyse in a unique framework both the failure and post-failure stages. Moreover, the numerical analyses indicate that the post-failure mechanisms are intimately tied to specific predisposing factors and boundary conditions, rather than to a single mechanical or state parameter of soil, such as for instance the soil relative density.

**Key words**: landslide; flow; failure; post-failure; acceleration; modelling

**(1) University of Salerno**
Lab. Geotechnics, Department of Civil Engineering
Via Ponte Don Melillo 1, 84084 Fisciano (SA), Italy

**(2) Universidad Politecnica de Madrid, Spain**
Department of Applied Mathematics and Computer Science
ETS Ingenieros de Caminos, UPM Madrid, Spain

## 1. Introduction

Landslides of the flow type still pose difficult challenges towards the combined geomechnical modelling of the failure and post-failure stages (Cascini et al., 2010) due to their mechanical characteristics. Particularly, the failure stage is characterized by the formation of a continuous shear surface through the entire soil mass (Leroueil, 2001) or, alternatively, plastic strains may affect a large amount of soil originating a so-called "diffuse" failure (Darve and Laoufa, 2000; Pastor et al., 2004); then, post-failure stage is represented by the rapid generation of large plastic strains and the consequent sudden acceleration of the failed soil mass (Hungr, 2004), often accompanied with a reduction of pore water pressures, which leads to a drastic increase of the landslide mobility. As a consequence, before failure onset, small soil deformations and displacements are measured (in coarse grained soils, soil deformations are even negligible) while at failure and during the post-failure stage, soil deformations rapidly increase up to some centimetres or metres. After that, the propagation stage occurs and displacements may attain values up to some kilometres, i.e. one or two orders of magnitude greater than the landslide source area dimension.

To date, valuable tools have been developed to model either failure (Leroueil, 2001; Pastor et al., 2007, Sanavia, 2009; among others) or propagation (McDougall & Hungr, 2004; Pastor et al., 2009; among others) and only few approaches (e.g. Pastor et al., 2002) refer to a unique mathematical framework to derive the governing equations which are then separately solved for analysing the triggering or propagation stage. The lack of a unified approach causes several difficulties and uncertainties in an appropriate hazard assessment related to a wide class of phenomena that can occur in both saturated and unsaturated conditions. To this regard, a good example is provided in figure 1 that shows a picture of two landslides occurred at Pizzo d'Alvano massif on May 1998 (Cascini et al., 2008); the first landslide (Fig. 1a) turned into a flow, later travelling about 1 km far; on the contrary, the second slide did not evolve into a landslide of the flow type and it was characterised by moderate displacements (Fig. 1b).

Considering the relevance of the topic, the present paper is aimed at proposing the use of new enhanced tools for geomechanical modelling. To this purpose, the available approaches for post-failure analysis are firstly discussed with some remarks proposed for both mechanical aspects and mathematical issues. Then, a hydro-mechanical coupled FEM model (Pastor et al., 1999, 2002) is shortly summarised and then proposed for modelling both the failure and post-failure stages within a unitary framework. Particularly, experimental

evidences derived from centrifuges tests are reproduced through a geomechanical modelling which is then extended to simple general slope schemes subjected to different water seepage conditions in both cases of loose and dense granular soils.

**Figure 1**

## 2. Literature review on post-failure stage

Post-failure stage is an outstanding topic since it discriminates different types of phenomena. In fact, it is quite evident that the chance for a landslide to achieve high velocities depends on: i) the initial acceleration of the failed mass and ii) subsequent transformation in a landslide of the flow type.

Anyway, the acceleration of the failed mass during the post-failure stage is associated to different mechanisms. Many Authors outline that the development of total or partial undrained conditions as the main cause of high pore-water pressures upon shearing. In particular, for loose unsaturated soils, volumetric collapse is discussed by Olivares & Damiano (2007), Yasufuku et al. (2005), Bilotta et al. (2006) and it is observed in constant-shear-drained triaxial tests upon wetting (Anderson and Riemer, 1995; Dai et al. 1999; Chu et al. 2003; Olivares & Damiano, 2007). For loose saturated soils, static liquefaction is introduced by Wang et al. (2002), Olivares & Damiano (2007), Van Asch et al. (2006) and observed in undrained triaxial tests (Lade 1992; Yamamuro and Lade 1998; Chu et al. 2003) as well as in undrained ring shear tests under controlled strain rates (Wang et al. 2002). Particularly, the build-up of pore pressures is shown to be relevant for soils having low density index (Eckersley 1990; Iverson 2000; Wang and Sassa 2001), fine grain size (Wang and Sassa 2003), low hydraulic conductivity (Iverson et al. 1997; Lourenco et al. 2006) and subjected to high deformation rate (Iverson et al. 1997).

The most of the above findings are obtained through laboratory tests such as isotropically consolidated undrained triaxial tests (ICU) (Chu et al., 2003), anisotropically consolidated undrained triaxial tests (ACU) (Eckersley, 1990), constant shear-drained triaxial tests (CSD) (Chu et al., 2003) even though strain localisation is more important under plane-strain or 3D conditions compared to triaxial conditions, as recently discussed by Wanatowski and Chu (2007, 2012). It is worth noting that all laboratory tests refer to idealized drainage conditions.

On the other hand, a direct measurement of pressures and displacements in real slopes is rare, indeed only possible for: i) monitored sites during the occurrence of landslides, ii) artificially induced failure in real slopes. In both cases, measurements are not repeatable.

Further insights derive from alternative approaches which are based on direct observation of pore water pressures and stresses in landslides artificially induced in slope models at a reduced scale (also called flume test). Through this approach, information can be obtained on failure and post-failure (Eckersley, 1990); however, these experiments are expensive and since they reproduce the real processes at a greatly reduced scale they may be irrespective of the full-scale slope behaviour. For instance, a large difference in stress levels may exist between model and prototype; in particular, the eventual capillary suction is out of proportion with its self-weight stress, allowing the model slope to remain steeper than would be possible at higher effective stress levels. Nevertheless, complex groundwater conditions, such as downward rainfall infiltration from ground surface and/or a downwards/upwards water spring from the bedrock to the tested soil layer, can be analysed through these tests (Lourenco et al., 2006)

A more recent approach is based on centrifuge tests which reproduce stress levels similar to those experienced by a real slope. Centrifuge tests - except for some drawbacks such as the high costs and the availability of sophisticated equipments - combine the advantages of highly instrumented slopes (such as full/reduced scale models) with the potential of geometrical configurations realistically reproducing the in-situ conditions. Particularly, Take et al. (2004) point out that the transition from slide to flow is caused by local failures producing a variation in the slope geometry. This mechanism is related to transient localized pore-water pressures that are not associated to the development of undrained conditions, but originated by the combination of particular hydraulic boundary conditions and stratigraphical settings. Experimental evidences show that the transition from slide to flow can occur both for loose and dense soils and it can also correspond to decreasing pore-water pressures during the post-failure stage. These results have been later confirmed also by other researchers through small-scale flume tests (Lourenco et al. 2006) or centrifuge tests (Lee et al., 2008, Ng, 2009; among others).

Based on previous considerations, mathematical modelling may be outlined as a powerful tool because, in principle, it can be used to investigate a wide variety of different scenarios even though the modelling of the post-failure stage is poorly addressed in the literature and the only available contributions refer to triggering

factors that differ from rainfall, such as earthquake (Pastor et al. 2004) and kinematic or static perturbations (Laouafa and Darve 2002). For this reason, the basic concepts of the used approach are hereafter summarised and then applied to different benchmark cases to estimate the reliability of the numerical modelling to reproduce well know experimental results.

## 3. Proposed methodology

### 3.1 Conceptual reference scheme

Based on well established experimental evidences from laboratory and centrifuge tests, Cascini et al. (2010) propose a conceptual reference scheme to point out some key differences among different types of landslides during their failure and post-failure stages. Particularly, referring to different types of post-failure stages, Cascini et al. (2010) outline the existence of three main classes of phenomena: i.e. slide, flowslide, slide to flow. Slide is a slope failure occurring under pore water drained conditions. On the other hand, a flowslide occurs when partially or totally undrained conditions develop and this is the typical case of loose saturated soil upon shearing (i.e. static liquefaction); flowslides are associated to the increase of pore water pressures. Finally, the transition from a slide to a flow is caused by local failures producing a variation in the slope geometry which, in turn, determines an unbalanced driving force; this corresponds to a sudden increase of deviatoric stress at almost constant effective mean pressures.

In the Authors' opinion, the features of the post-failure stage are strictly tied to the failure type and, in principle, the two stages should be analysed with a unitary approach. Moreover, the value attained by pore water pressures during the post-failure stage is a key issue for engineering purposes since it determines the soil mobility during the subsequent propagation stage. Therefore, some insights are hereafter proposed to individuate typical scenarios corresponding to the development of high pore water pressures in simple general slope schemes subjected to groundwater rainfall infiltration. It is important noting that a suitable approach should allow properly considering the twofold issue of Representative Elementary Volume (REV) and slope scale, particularly, i) the soil mechanical behaviour at REV scale, also including liquefaction phenomena and ii) at slope scale, the geometry constraints which predispose the failure and the hydraulic boundary conditions which determine the different triggering mechanisms.

141

142 **3.2 Mathematical model**

143 The adopted hydro-mechanical coupled model mainly derives from the fundamental contribution of
144 Zienkiewicz at al. (1980, 1999) that considers a solid skeleton and two fluid phases, water and air, which fills
145 the voids. The skeleton is made of particles of density $\rho_s$ with porosity $n$ (volume percent of voids in the
146 mixture) and void ratio $e$ (volume of voids per unit volume of solid fraction). Movement of the fluid is
147 considered as composed of two parts, the movement of soil skeleton and motion of the pore water relative to
148 it. The total stress tensor acting on the mixture can be decomposed as the sum of an effective stress tensor σ'
149 acting on soil skeleton and a hydrostatic pore pressure term $p_w$ which for unsaturated soils with zero air
150 pressure corresponds to the averaged pore pressure $\overline{p} = S_r p_w$.

151 The governing equations of the model are reported in Cascini et al. (2010) and they consist in: i) balance
152 of momentum equation for the mixture, ii) balance of mass of the pore water, iii) mass conservation for the
153 pore fluid and iv) balance of momentum of the pore fluid. Those equations have to be complemented by a
154 kinematic relation linking velocities to rate of deformation tensor, and a suitable constitutive model. The
155 latter is the Pastor-Zienkiewicz (PZ) model which is suitable to accurately describe the behaviour of either
156 loose or dense granular soils, both in drained and undrained conditions, along complex stress paths. In the PZ
157 model, derived from the theoretical fundamentals of the Generalised Plasticity Theory (Pastor et al., 1990), it
158 is assumed that plastic deformations may occur upon either loading or unloading and they are derived
159 without the need to define the: i) yielding surface, ii) plastic potential surface, iii) consistency law. In details,
160 the model is completely defined once the following quantities are fixed: i) three directions (load direction
161 $n_{gL}$, unload direction $n_{gU}$ and neutral load direction n), ii) two scalars (plastic moduli $H_L$ and $H_U$) and iii) the
162 elastic tensor $D_e$. Globally, 12 parameters are defined ($K_{ev0}$, $G_0$, $M_g$, $M_f$, $H_0$, $H_{u0}$, $\alpha_g$, $\alpha_f$, $\beta_1$, $\beta_0$, $\gamma$, $\gamma_u$); $K_{ev0}$ and
163 $G_0$ are, respectively, the bulk modulus and shear modulus, $M_g$ and $M_f$ represent in the q-p' space the slope
164 of critical state line and the slope of instability line (Chu et al., 2003), $H_0$ and $H_{u0}$ are hardening
165 modulus in loading and unloading. Calibration of these parameters can be performed through standard
166 triaxial tests according to the procedures indicated by Zienkiewicz et al. (1999) who also provide the values
167 of some constants incorporated in the model, named $\alpha_g$, $\alpha_f$, $\beta_1$, $\beta_0$, $\gamma$ and $\gamma_u$. It is worth noting that $M_f$ is
168 univocally related to the soil relative density as suggested by Pastor et al. (1990). The governing equations of

the hydro-mechanical coupled model are implemented in the FEM code named "GeHoMadrid FEM" whose details reported in Pastor et al. (1999, 2002).

## 4. Testing the proposed approach

### 4.1. Benchmarks at REV scale

The hydro-mechanical response of a soil specimen during undrained triaxial tests is here simulated referring to the experiments of Eckersley (1990). The mechanical parameters are reported in Table 1 and they are calibrated referring to the procedure suggested by Zienkiewicz et al. (1999). Figure 2 shows the achieved results which match the experimental evidences; particularly, it can be reproduced either a strain-softening behaviour corresponding to the static liquefaction (very loose curve) or a strain-hardening soil response (very dense curve) which is typical of saturated dense sands upon undrained triaxial stress paths. The capability of the model to discriminate between the different behaviour of loose and dense soils is also outlined in figure 2c that shows the mean effective stress vanishing as the equivalent plastic strain ($\varepsilon_{eq}^{p} = (2/3 \cdot e^{p} : e^{p})^{1/2}$) increases in the case of "loose soil" while the opposite for "dense soil". The results of the simulated undrained triaxial tests are used as a reference case for discussion.

**Table 1**

**Figure 2**

### 4.2. Benchmarks from centrifuge tests

**Experimental evidence and Limit Equilibrium Analysis**

Moving from REV to slope scale, it is important to individuate simple general benchmarks to be referred with either standard or advanced approaches.

In the tests performed by Take et al. (2004), the slope configuration of figure 3a is used consisting in a layered shallow deposit 33° inclined over impervious bedrock. Due to permeability differences (coarser layer soils are more permeable than the upper ones), and imposed hydraulic boundary conditions (consisting in a water spring at the upper right corner of the model), transient groundwater seepage is observed in both layers and at the toe of the slope model.

In the experiments, due to the increase of pore water pressures, a slope failure occurs and the sudden acceleration of the failed mass is measured for both cases of loose and dense soils (Fig. 3b). From the experimental evidences, it can be outlined the existence of different stages of the observed landslides. It is worth noting that the acceleration of the failed mass (i.e. post-failure stage) corresponds to the decrease of pore water pressures, mainly due to a concurrent modification of slope geometry (Fig. 3c).

**Figure 3**

To investigate the potential of standard tools, such as Limit Equilibrium Methods (LEMs), to adequately reproduce the above mentioned centrifuge tests, a proper set of scale relationships is taken into account between the centrifuge model (Fig. 3) and the equivalent prototype (Fig. 4a); scale relationships are related to the acceleration factor N used in the centrifuge tests. Consequently, the equivalent prototype is characterized by time and length scales multiplied by N while mechanical properties (eg. friction angle and permeability) and pressure/stress levels are equal to those acting during the tests. In their experiments Take et al. (2004) use a factor N equal to 30 and the equivalent prototype is shown in figure 4a and it reproduces the upper coarser soil layer of the centrifuge model. Take et al. (2004) also provide information on both groundwater conditions observed at failure onset and soil mechanical properties; the latter ones were also investigated through laboratory experiments described in GEO (1999) and Ng et al. (2004).

The limit equilibrium analyses are developed using the methods of Janbu (1954) and Morgenstern and Price (1965). The achieved results show that the slip surface with the minimum factor of safety individuates a soil volume which strictly corresponds to the highest values of the displacement field measured during the experiments (Fig. 4b). In conclusion, this simplified approach allows interpreting somehow the experimental results and it also outlines the severity of slope geometry and hydraulic boundary conditions which cause a strong reduction of the safety factor; however, it is not possible to provide any distinction between the case of loose and dense soil.

**Figure 4**

## Hydro-mechanical coupled stress-strain analyses

The same centrifuge tests are here analysed using the proposed mathematical approach (sect. 3) and referring to the definitions of failure and post-failure given in section 1. In the numerical analyses an unstructured mesh is used with triangular elements on average not larger than 0.4 m. Adequate kinematic and hydraulic boundary conditions are selected to best reproduce the conditions imposed during the tests (Fig. 5). Particularly, a null pore water pressure values is assumed at point E - corresponding to the water table level observed at failure during the tests - to reproduce the raising of the water table in the upper soil layer. In the FEM analysis, pore water pressure is allowed to change in space and time, starting from an initial value of -5kPa throughout the slope model. This is adequately taken into account referring to Bishop's stresses (for details see Pastor et al., 2002, 2007). However, for sack of simplicity, numerical analyses are performed in the hypothesis of fully saturated conditions and the used version of the PZ constitutive model fits this hypothesis. Of course, the analyses could be extended to the case of unsaturated conditions but this is beyond the scope of the present paper.

The soil mechanical properties are reported in table 2 and they are either taken from GEO (1999), Ng et al. (2004) and Take et al. (2004), e.g. $\gamma_{sat}$, n, $M_g$ and $M_f$, or indirectly estimated/calibrated, e.g. $k_{sat}$, E, $\eta$, $H_0$, comparing the experimental evidences and the numerical results. It is worth noting that in table 2 different values of $M_f$ are assumed which derive from different values of relative soil density while the same critical friction angle ($M_g$) and bulk modulus ($K_{ev0}$) are considered for both loose and dense soils. This strong assumption is aimed at emphasizing in a limit case the role played by soil porosity as a fundamental factor for slope behaviour upon failure and beyond.

Hydro-mechanical coupled quasi-static analyses are performed to take into account the coupling between the solid skeleton and pore fluid. Numerical results and experimental evidences are compared referring to the following quantities: i) "equivalent centrifuge" times ($t_{centr}$), i.e. times relative to the prototype (numerical model) divided by the factor N, wich can be directly compared with those measured in centrifuge tests, ii) "centrifuge" displacements ($displ_{centr}$) computed in the same way, iii) pore water pressures and effective stresses as computed from the numerical modelling.

**Figure 5**

**Table 2**

Simulated plastic strains significantly differ in the case of loose and dense soil (Fig. 6) for both the value (larger for loose soil) and extent of the affected zone. In the case of loose soil, "diffuse" plastic strains are simulated, firstly at the toe of the slope (Fig. 6a), and then they involve a larger amount of the slope as time elapses. For dense soil (Fig. 6b), plastic strains appear firstly at the toe of the slope and then they are "localized" along a slip surface where plastic strains accumulate as the process evolves. The above mentioned differences depend only on the soil relative density values since all the other soil mechanical properties are assumed equal in the two cases. However, apart from the different type of failure, i.e. diffuse or localized, a different time evolution is also outlined (Fig. 7a). For loose soil, the failure stage is shorter because higher excess pore water pressures rapidly accumulate in the slope until it fails. Conversely, in the case of dense soil, both the pre-failure stage (mainly corresponding to elastic strains) and the failure stage are longer in time. These differences are also evidenced by the computed stress-paths and displacements in figure 7c and 7d. Globally, a slower slope response is observed for dense soil and this result completely agrees the experimental evidences of figure 3b. These results are further validated observing that in figure 3c pore water pressures are decreasing after failure in both cases; this process is reproduced in figure 7b.

Indeed, minor mismatches among the experimental and numerical results can be outlined: i) for dense soil, stiffer slope behaviour is outlined in the centrifuge test rather than in the numerical model (Fig. 3b and Fig 7d), ii) at failure, higher pore water pressures are simulated for dense soil rather than for loose soil. Regarding the former aspect, it must be noted that different stiffness values could be easily estimated and introduced in the numerical analyses for dense and loose soils (while they are assumed as equal); differently, the comparison of the obtained results for dense and loose soils could be confusing if not misleading. For the same reason, an equal soil conductivity is assumed for both cases of dense and loose soils; assuming a lower soil conductivity for dense soil, higher pore water pressure could be simulated. It is worth noting that the used model also correctly capture the onset of a yielding zone in the upper right corner, as shown by Lee et al. (2008).

As for the post-failure stage, it is of interest to note that, independently from the value of soil relative density, the failed mass accelerates (Fig. 7d), pore water pressure decrease as, respectively, evidenced by the experimental tests (Figures 3b and 3c).

**Figure 6**

**Figure 7**

## 5. New insights on post-failure stage

In order to evaluate the novelty and potentialities of the proposed approach compared to a uncoupled approach, two simple benchmarks at slope scale are hereafter analysed comparing the standard limit equilibrium analyses with hydro-mechanical coupled stress-strain analyses.

Particularly, the slope is composed of a homogeneous saturated soil being 10m high and 27° steep and it is subjected to two different quasi steady-state groundwater seepage conditions, i.e. sub-horizontal (case1) and vertical downwards directed (case 2), which are referred as limit cases of real seepage conditions in the final discussion. Soil mechanical properties are given in figure 8 and it is worth mentioning that a small cohesion (1kPa) is considered in all the numerical simulations to prevent local superficial failures which are not of interest in the paper being related to the steep slope geometry,.

For case 1 (sub-horizontal seepage), the imposed hydraulic boundary conditions are: 1) an increasing water total head from 5 to 15 m at point A of figure 8, 2) a maximum pore water pressure equal to zero at slope surface, 3) pore water pressure equal to zero at boundary DE. Consequently, at the initial stage, a uniform field of nil pore water pressure is assumed, corresponding to a unity gradient seepage downwards; then, the water table is kept raising and the head isolines becoming somehow vertical and correspondingly the seepage velocities become quasi-horizontal. This leads to a general increase of pore water pressures in the whole slope up to failure onset.

For case 2 (sub-vertical seepage), the slope is subjected to a vertical groundwater seepage due to the following hydraulic boundary conditions: i) lateral boundaries impervious, ii) nil pore water pressures applied to the whole ground surface, iii) an imposed pore water pressures at the lower boundary (0 kPa at the initial stage, later increasing up to 20 kPa with a increment rate of $7e^{-3}$ kPa/s). Therefore, the infiltration velocities are always vertical; the hydraulic gradient is slowed down while pore water pressure values are increased in the slope due to the hydraulic boundary condition at the bottom of the slope.

**Figure 8**

### 5.1. Limit equilibrium analyses

The results achieved through an uncoupled approach (Cascini et al., 2010) are based on a seepage analysis first and limit equilibrium analyses later. Pore water pressures are computed through the commercial code SEEP/W (Geoslope, 2005) and in figure 9 the isolines of total water head are shown at the final step of the analysis; pore water pressures are used as input data for limit equilibrium analyses performed through the methods of Morgenstern & Price (1965) and Janbu (1954) by using the SLOPE/W code (Geoslope, 2005). Several slip surfaces are considered with different shapes and depths and their safety factors are tracked with reference to the computed pore water pressures.

For case 1, due to a generalised increase of pore water pressures, factor of safety of the slope decreases in time from the initial value 1.65 up to 1. Particularly, the critical slip surface corresponds to the toe of the slope where high pore water pressures arise, thus drastically reducing the soil shear strength. For case 2, the initial value of safety factor is higher (1.8) and it decreases less than in the previous case up to the final value 1.6; failure is not predicted in this case.

In conclusion, the standard uncoupled limit equilibrium approach only outlines the importance of the groundwater regime for the attainment of limit equilibrium conditions in these two cases which are characterised by the same slope geometry.

**Figure 9**

### 5.2 Hydro-mechanical coupled stress-strain analyses

For both cases of figure 9, stress-strain analyses are performed referring to an unstructured mesh which is composed of 698 triangular elements, with 6 nodes each; the dimensions of the triangular elements are not larger than 2m and time steps of about 1s; the soil mechanical parameters of table 3 are used.

In the case of a sub-horizontal seepage condition (case 1), the results of stress-strain analysis outline that contours of the equivalent plastic strains and their value depend on soil density. For loose soil, plastic deformations concentrate along a slip surface, thus causing a triggering mechanism for a landslide (Fig. 10). For dense soil, plastic deformations only partially affect the toe of the slope while not causing a soil volume to be mobilized (Fig. 10). The different deformation modes affect the time evolution of the equivalent plastic strains (Fig. 10) and important differences can be observed when $p'/p_0$ (ratio of the mean effective pressure to its initial value) is plotted versus the equivalent plastic strain (Fig. 10). In fact, for loose soil, $p'/p_0$ reduces

up to 20% while a lower reduction is simulated in the case of dense soil; accordingly, failure is simulate for loose soils while not for dense soils.

Comparing these results with those of LEM analyses for case1, it comes out that both methods allow assessing the onset of failure. However, important differences are also outlined: i) FEM analyses provide a mobilized mass larger than LEM in the case of loose soils, ii) LEM is a conservative approach for the case of dense soil. It is convenient observing that the comparison of LEM and stress-strain FEM analyses is difficult to justify from a theoretical viewpoint, since LEM disregards non-associate flow rule and soil deformations. However, this comparison is meaningful for engineering purposes as both approaches provide the mobilized soil volume that can be quantitatively compared in the framework of engineering forecasting analyses. In addition, the comparison of LEM and FEM outlines the accuracy of LEM for different slope geometries and head water contours.

**Table 3**

**Figure 10**



Stress-strain analyses for the case of loose soil and sub-vertical groundwater seepage (case 2 of figure 9) show that pore water pressures increase due to the slope deformation; it is interesting noting that a large soil volume achieves high values of pore water pressures which cause the slope failure according to a diffuse mode (Fig. 11). Unlike the previous case of figure 8, pore water pressures undergo a generalised increase due to the soil response at REV scale; therefore, a large soil volume is involved in the slope failure. This generalised increase of pore water pressures does not require the effective mean stress p' to reach a very low value and failure is achieved when $p'/p_0$ reduces reach 60% (Fig. 11). Conversely, in the case of dense soils, failure is not simulated despite the same hydraulic boundary conditions have been applied (Fig. 11).

Comparing FEM and LEM results of case 2 and based on previous comments, it is not surprising to note that using LEM the safety factor is always higher than one (in both case of loose and dense soil) due to the drastic simplification made at REV scale in the LEM analysis. Conversely, coupled FEM analysis allows: i) accounting for a more realistic description of soil behaviour at REV scale and ii) adequately simulating the failure onset and post-failure stage that are both depending on soil density.

**Figure 11**

362

363 **5.3 Discussion of the numerical results**

364 An effort to provide some general results is here devoted to the analysis of pore water pressures
365 variations during the failure and post-failure stages. Particularly, for all the above mentioned cases
366 (soil REV, centrifuge tests and slope benchmarks), the achieved results are plotted with reference to
367 two adimensional quantities: i) $\varepsilon_{pl}/\varepsilon_{pl}^{max}$, i.e. the ratio of equivalent plastic strains to its maximum
368 value during the analysis and ii) $p'/p'_0$, the ratio of the mean effective stress to its initial value, later
369 named normalized p' (Fig. 12). This variable $p'/p'_0$ has been formerly used by Pastor et al. (2007)
370 for detecting via numerical modelling the occurrence of soil liquefaction due to earthquake and it is
371 thought to be a useful factor to differentiate among distinct slope response to the applied hydraulic
372 boundary conditions.

373 For the dense soil specimen the normalized p' decreases first and later increases, during the
374 failure stage, accompanied with a very small strain rate; in such a case, this is the only failure mode
375 compatible to the combination of soil mechanical features and imposed boundary conditions to
376 stresses and pore pressures (i.e. undrained triaxial loading). In all the remaining cases, $p'/p'_0$
377 decreases while failure is approaching. Particularly, for the loose soil specimen a very low value of
378 $p'/p'_0$ is reached because there isn't any possibility for the specimen to somehow react against the
379 imposed boundary conditions. Different patterns are drawn for centrifuge tests which, at point P of
380 figure 5, exhibit first a drastic reduction of $p'/p'_0$ (failure stage) due to the severe slope geometry
381 and then a moderate increase of $p'/p'_0$ (during the post-failure stage) mainly due to a change of
382 slope geometry and consequent increase pore water pressure; this behaviour is more exacerbated for
383 loose than dense soils. Whereas, a gradual reduction of $p'/p'_0$ is modelled at point P of figure 8, for
384 the case of quasi-horizontal seepage with the lowest value reached for loose soil. Finally, for the
385 case of quasi-vertical seepage, a different slope behaviour is simulated with a reduction of $p'/p'_0$ for
386 loose soils but not for dense soils. In conclusion, an important mutual interplay among soil REV
387 response, stress conditions (plane-strain or axial symmetric), slope geometry and hydraulic

boundary conditions is shown; this interplay really determines the global slope behaviour.

**Figure 12**

## 6. Concluding remarks

The application of the proposed methodology to both centrifuge evidences and two simple benchmarks highlights some general insights. Particularly, it is shown that the slope response is controlled by two different "driving mechanisms": i) the generation of excess pore water pressures, and ii) localization of plastic strains. The former mechanism is typical of loose saturated sands and it controls the soil behaviour at REV scale; in fact, for loose soils, high pore water pressures are simulated also due to soil deformation. The latter mechanism is typical of dense soils and it is acting at slope scale; in this sense, the chance for localised strains to develop depend on: i) slope geometry (steep slope), ii) stress conditions (plain-strain rather than triaxial) and iii) local boundary conditions (groundwater impoundments) that enhance the local generation of high plastic strains and the subsequent development of a slip surface.

Based on the achieved results it is outlined that: i) in the practical applications the case of loose soils must be surely taken into account for the possible failure and post-failure stage scenarios, ii) the case of dense soils also deserves a special attention because, depending on slope geometry and boundary conditions, it may correspond to scenarios of brittle localised failures which imply a sudden acceleration of the failed mass which cause a slide to turn into a flow.

## Acknowledgements

The authors would like to dedicate this paper to the memory of the recently departed Prof. Giuseppe Sorbino. His vitality, optimistic nature, and many other human and scientific qualities will be very much missed.

## Figure captions

**Figure 1.** Examples of landslides occurred at Pizzo d'Alvano massif on May 1998: a) slides evolved into a landslide of the flow type; b) in the same are, an example of slide not evolved into a flow.

**Table 1.** Parameters of the constitutive Pastor-Zienkiewicz (PZ) model used for simulating the experiments of Eckersley (1990).

**Figure 2.** Mechanical behaviour of loose and dense soils used by Eckersley (1990): a) experimental evidence, b) numerical results, c) computed equivalent plastic strain versus ratio of mean effective stress to its initial value.

**Figure 3.** Observed behaviour of centrifuge slope model for loose and dense soils: a) centrifuge model, b) displacement measured at PIV1, c) pore water pressures measured at PPTT1 (modified from Take et al., 2004).

**Figure 4.** a) Results of limit equilibrium analysis, b) comparison between the computed critical slip surface and the experimental evidence from Take et al. (2004).

**Figure 5.** Slope scheme used for the numerical analyses.

**Table 2.** Soil mechanical parameters for simulation of centrifuge test.

**Figure 6.** Time evolution of equivalent plastic strains computed for loose and dense soil (case "L" and "D" of table 2).

**Figure 7.** Results for the node P of figure 5: a) equivalent plastic strains, b) pore water pressures, c) stress path in the p'-q plane, d) horizontal displacements versus time.

**Figure 8.** New slope benchmarks to test the proposed approach.

**Figure 9.** Results of limit equilibrium analyses for slope benchmarks: case 1(a), case 2 (b).

**Table 3.** Soil mechanical parameters of slope shown in figure 9.

**Figure 10.** Results of numerical analyses for the case of sub-horizontal seepage (case 1).

**Figure 11.** Results of numerical analyses for the case of sub-vertical seepage (case 2).

**Figure 12.** Ratio of equivalent plastic strain to its maximum value (x-axis) versus the ratio of mean effective pressure to its initial value (y-axis) for different analyzed cases.

## 7. References

1. Anderson, S.A and Riemer. M.F., 1995. Collapse of saturated soil due to reduction in confinement. Journal of Geotechincal Engineering ASCE 121 2, 216-220.
2. Bilotta, E., Foresta, V. and Migliaro, G. 2006. Suction controlled laboratory tests on undisturbed

pyroclastic soil: stiffnesses and volumetric deformations. Proc. International Conference on Unsaturated Soils, 2-6 April, Carefree, Arizona USA, 1, 849-860

3. Cascini, L., Cuomo, S. and Guida, D. 2008. Typical source areas of May 1998 flow-like mass movements in the Campania region, Southern Italy. Engineering Geology, 96, 107-125.

Cascini, L., Cuomo, S., Pastor, M. and Sorbino, G. 2010. Modelling of rainfall-induced shallow landslides of the flow-type. ASCE's Journal of Geotechnical and Geoenvironmental Engineering, 1, 85-98.

Chu, J., Leroueil, S., and Leong, W. K. 2003. Unstable behaviour of sand and its implications for slope instability. Canadian Geotechnical Journal, 40, 873-885.

4. Dai, F., Lee, C.F., Wang, S. and Feng Y. 1999. Stress-strain behaviour of a loosely compacted volcanic-derived soil and its significance to rainfall-induced fill slope failures. Engineering Geology, 53, 359-370.

5. Darve, F. and Laouafa F. 2000. Instabilities in granular materials and application to landslides. Mechanics of Cohesive frictional Materials, 58, 627-652.

6. Eckersley D. 1990. Instrumented laboratory flowslides. Géotechnique, 40, 489-502.

7. Geotechnical Engineering Office (1999) Slope No. 11NW-B/FR61, Beacon Hill Radar Airport Station, Final Laboratory Testing Report, Geotechnical Engineering Office, Civil Engineering Department, The Government of the HKSAR.

8. Geoslope 2005. User's guide. GeoStudio 2004, Version 6.13. Geo-Slope Int. Ltd. Calgary, Canada.

9. Hungr, O. 2004. Flow slides and flows in granular soils. Proc. of the Int. Workshop Flows 2003 - Occurrence and Mechanisms of Flows in Natural Slopes and Earthfill, Sorrento, Patron Ed..

10. Iverson 2000. Landslide triggering by rain infiltration. *Water Resources Research*, 367, 1897-1910.

11. Iverson, R.M., Reid, M.E. and LaHusen R.G. 1997. Debris flow mobilization from landslides. Annual Review Earth Planet. Science, 25, 85-138.

12. Janbu, N. 1954. Application of Composite Slip Surface for Stability Analysis. European Conference on Stability Analysis, Stockholm, Sweden.

13. Lade, P.V. 1992. Static instability and liquefaction of loose fine sandy slopes. Journal of Geotechnical Engineering ASCE, 118 1, 51-71.

14. Laouafa, F. and Darve F. 2002. Modelling of slope failure by a material instability mechanism.

Computers and Geotechnics, 29, 301-325.

15. Lee, Y.S., Cheuk, C.Y., and Bolton, M.D. (2008) Instability caused by a seepage impediment in layered fill slopes. Canadian Geotechnical Journal, 45(10), 1410-1425.
16. Leroueil S. 2001. Natural slopes and cuts: movement and failure mechanisms. Geotechnique, 51, 3, 197-243.
17. Lourenco, S., Sassa, K. and Fukuoka, H. 2006. Failure process and hydrologic response of a two layer physical model: Implications for rainfall-induced landslides. Geomorphology, 731-2, 115-130.
18. McDougall, S., Hungr, O., 2004. A model for the analysis of rapid landslide motion across three-dimensional terrain. Canadian Geotechnical Journal, 41, 1084-1097.
19. Morgenstern, N.R. and Price, V.E. 1965. The analysis of the stability of general slip surfaces. Geotechnique, 151, 79-93.
20. Ng CWW, Fung WT, Cheuk CY, Zhang L (2004) Influence of stress ratio and stress path on behaviour of loose decomposed granite. ASCE Journal of Geotechnical and Geoenvironmental Engineering 130(1): 36-44.
21. Ng, C.W.W. 2009. What is Static Liquefaction Failure of Loose Fill Slopes? In: The first Italian Workshop on Landslides Napoli 8-10 giugno 2009 NAPOLI Doppiavoce. Studio editoriale Vol.1, pp. 43-51 ISBN:9788889972120
22. Olivares, L. and Damiano, E. 2007. Postfailure Mechanics of Landslides: Laboratory Investigation of Flowslides in Pyroclastic Soils. Journal of Geotechnical and Geoenvironmental Engineering ASCE, 1331, 51-62.
23. Pastor M., Fernández Merodo J.A., Herreros M.I., Mira P., González E., Haddad B., Quecedo M., Tonni L. Drempetic V. 2007. Mathematical,Constitutive and Numerical Modelling of Catastrophic Landslides and Related Phenomena. Rock Mechanics and Rock Engineering, 411, 85-132
24. Pastor, M., Fernandez-Merodo, J.A., Gonzalez, E., Mira, P., Li, T. and Liu, X. 2004. Modelling of landslides: I. Failure mechanisms. Degradations and Instabilities in Geomaterials, CISM Course and Lectures No. 461, Darve F. and Vardoulakis I. ed., Springer-Verlag, 287-317.
25. Pastor, M., Haddad, B., Sorbino, G., Cuomo, S. and Drempetic, V. 2009. A depth-integrated, coupled SPH model for flow-like landslides and related phenomena. Int. J. Numer. Anal. Meth. Geomech 33:

143-172.

26. Pastor, M., Li, T., Liu, X. and Zienkiewicz, O.C. 1999. Stabilized low order finite elements for failure and localization problems in undrained soils and foundations. Comput. Methods Appl. Mech. Engrg. 174, 219-234.
27. Pastor, M., Quecedo, M., Fernandez-Merodo, J.A., Herreros, M.I., Gonzalez, E. and Mira P. 2002. Modelling tailing dams and mine waste dumps failures. Geotechnique, 528, 579-591.
28. Pastor, M., Zienkiewicz, O.C. and Chan, A.H.C. 1990. Generalized plasticity and the modelling of soil behaviour. Int. J. Numer. and Anal. Methods in Geomechanics, 14, 151-190.
29. Sanavia, L. 2009. Numerical modelling of a slope stability test by means of porous media mechanics. Engineering Computations (Swansea, Wales) 26 (3), 245-266.
30. Take, W.A., Bolton, M.D., Wong, P.C.P. and Yeung F.J. 2004. Evaluation of landslide triggering mechanisms in model fill slopes. Landslides, 1, 173-184.
31. Van Asch, Th.W.J. , Malet, J.P. and van Beek L.P.H. 2006. Influence of landslide geometry and kinematic deformation to describe the liquefaction of landslides: Some theoretical considerations. Engineering Geology, 88, 59-69.
32. Wang, F.W., Sassa, K. and Wang G. 2002. Mechanism of a long-runout landslide triggered by the August 1998 heavy rainfall in Fukushima Prefecture, Japan. Engineering Geology, 63, 169-185.
33. Wang, G. and Sassa K. 2001. Factors affecting rainfall induced landslides in laboratory flume tests. Géotechnique, 51, 587-600.
34. Wang, G. and Sassa, K. 2003. Pore-pressure generation and movement of rainfall-induced landslides: effects of grain size and fine-particle content. Engineering Geology, 69, 109-125.
35. Yamamuro, J.A. and Lade P.J. 1998. Steady-state concepts and static liquefaction of silty sands. ASCE J Geotech Geoenviron Eng, 1249, 868-878.
36. Yasufuku, N., Ochiai, H. and Hormdee, D. 2005. An empirical relationship for evaluating collapsible settlements of volcanic ash sandy soil. Advanced experimental unsaturated soil mechanics. Tarantino, Romero and Cui ed., 265-272.
37. Zienkiewicz, O.C., Chan, A.H.C., Pastor, M., Shrefler, B.A. and Shiomi T. 1999. Computational Geomechanics. J.Wiley and Sons.

528 38. Zienkiewicz, O.C., Chang C.T. and Bettess P. 1980. Drained, undrained, consolidating dynamic
529 behaviour assumptions in soils. Geotechnique, 30, 385-395.

**Figure 1.** Examples of landslides occurred at Pizzo d'Alvano massif on May 1998: a) slides evolved into a landslide of the flow type; b) in the same are, an example of slide not evolved into a flow.


Examples of landslides occurred at Pizzo d'Alvano massif on May 1998: a) slides evolved into a landslide of the flow type; b) in the same are, an example of slide not evolved into a flow.
190x142mm (300 x 300 DPI)

**Figure 2.** Mechanical behaviour of loose and dense soils used by Eckersley (1990): a) experimental evidence, b) numerical results, c) computed equivalent plastic strain versus ratio of mean effective stress to its initial value.

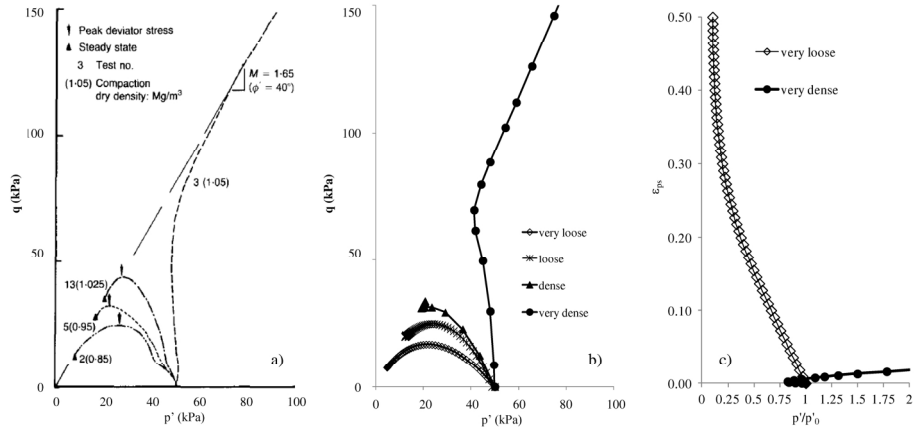


Mechanical behaviour of loose and dense soils used by Eckersley (1990): a) experimental evidence, b) numerical results, c) computed equivalent plastic strain versus ratio of mean effective stress to its initial value.
190x142mm (300 x 300 DPI)

**Figure 3.** Observed behaviour of centrifuge slope model for loose and dense soils: a) centrifuge model, b) displacement measured at PIV1, c) pore water pressures measured at PPTT1 (modified from Take et al., 2004).

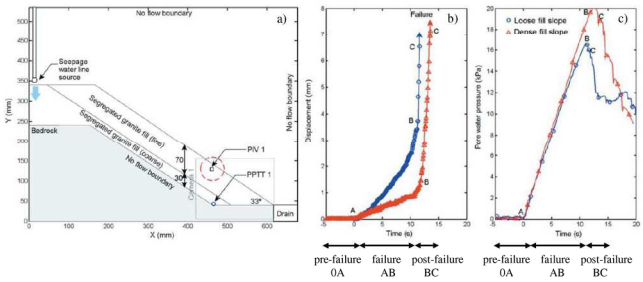


Observed behaviour of centrifuge slope model for loose and dense soils: a) centrifuge model, b) displacement measured at PIV1, c) pore water pressures measured at PPTT1 (modified from Take et al., 2004).
190x142mm (300 x 300 DPI)

**Figure 4.** a) Results of limit equilibrium analysis, b) comparison between the computed critical slip surface and the experimental evidence from Take et al. (2004).

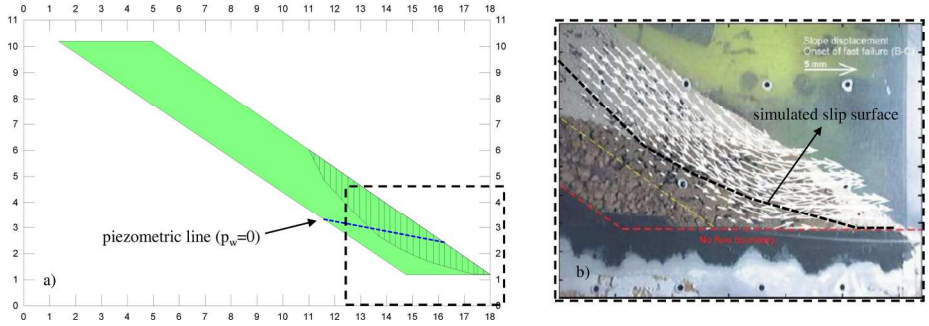


a) Results of limit equilibrium analysis, b) comparison between the computed critical slip surface and the experimental evidence from Take et al. (2004).
190x142mm (300 x 300 DPI)

**Figure 5.** Slope scheme used for the numerical analyses.

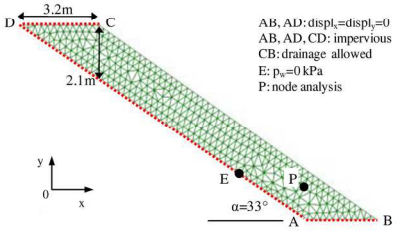


Slope scheme used for the numerical analyses.
190x142mm (300 x 300 DPI)

**Figure 6.** Time evolution of equivalent plastic strains computed for loose and dense soil (case "L" and "D" of table 2).

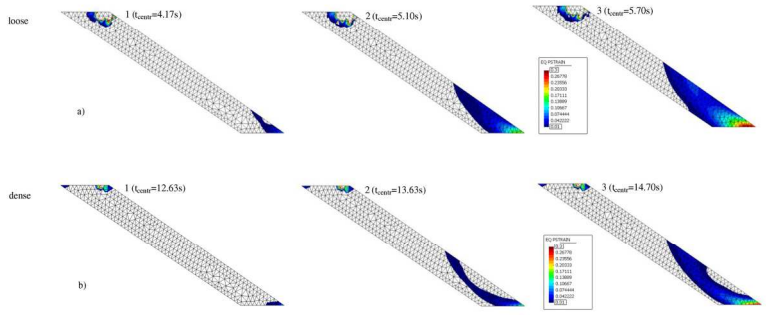


Time evolution of equivalent plastic strains computed for loose and dense soil (case "L" and "D" of table 2).
190x142mm (300 x 300 DPI)

**Figure 7.** Results for the node P of figure 5: a) equivalent plastic strains, b) pore water pressures, c) stress path in the p'-q plane, d) horizontal displacements versus time.

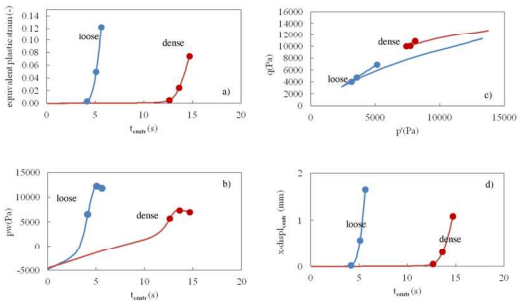


Results for the node P of figure 5: a) equivalent plastic strains, b) pore water pressures, c) stress path in the p'-q plane, d) horizontal displacements versus time.
190x142mm (300 x 300 DPI)

**Figure 8.** New slope benchmarks to test the proposed approach.

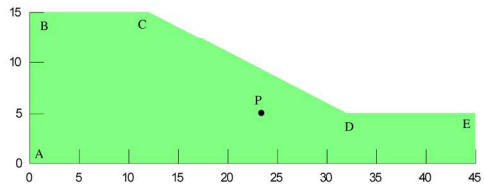


New slope benchmarks to test the proposed approach.
190x142mm (300 x 300 DPI)

**Figure 9.** Results of limit equilibrium analyses for slope benchmarks: case 1(a), case 2 (b).

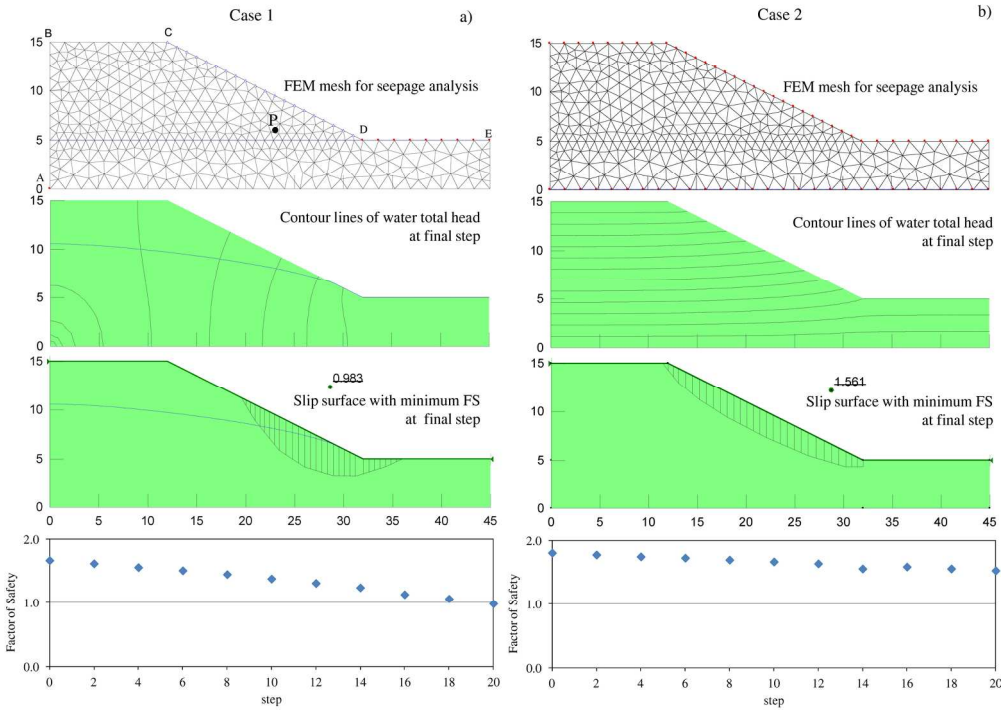


Results of limit equilibrium analyses for slope benchmarks: case 1(a), case 2 (b).
190x142mm (300 x 300 DPI)

**Figure 10.** Results of numerical analyses for the case of sub-horizontal seepage (case 1).

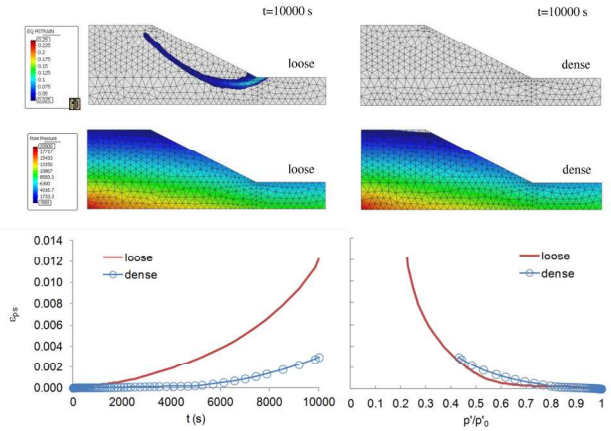


Results of numerical analyses for the case of sub-horizontal seepage (case 1).
190x142mm (300 x 300 DPI)

**Figure 11.** Results of numerical analyses for the case of sub-vertical seepage (case 2).

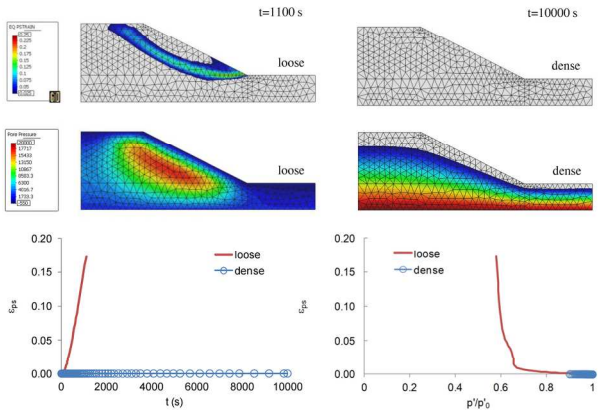


Results of numerical analyses for the case of sub-vertical seepage (case 2).
190x142mm (300 x 300 DPI)

**Figure 12.** Ratio of equivalent plastic strain to its maximum value (x-axis) versus the ratio of mean effective pressure to its initial value (y-axis) for different analysed cases.

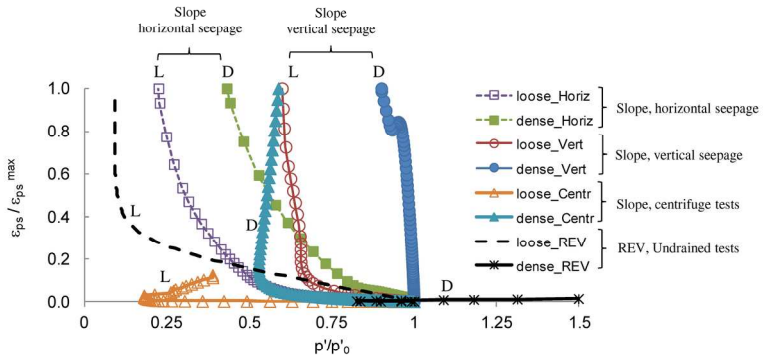


Ratio of equivalent plastic strain to its maximum value (x-axis) versus the ratio of mean effective pressure to its initial value (y-axis) for different analyzed cases.
190x142mm (300 x 300 DPI)

Table 1

| Case | $\gamma_s$ (kN/m$^3$) | e (-) | $D_r$ (-) | $\sigma'_{33}$ (kPa) | $K_{ev0}$ (kPa) | $G_0$ (kPa) | $M_g$ (-) | $M_f$ (-) | $H_0$ (-) | (*) |
|---|---|---|---|---|---|---|---|---|---|---|
| very loose | 12.7 | 0.50 | 0.47 | 50 | $3.3 \cdot e^4$ | $2.0 \cdot e^4$ | 1.636 ($\varphi$=40°) | 0.772 ($\varphi_{IL}$=20°) | $1 \cdot e^{-2}$ | |
| loose | 13.4 | 0.43 | 0.58 | 50 | $3.7 \cdot e^3$ | $2.2 \cdot e^3$ | 1.636 ($\varphi$=40°) | 0.941 ($\varphi_{IL}$=24°) | 15 | |
| dense | 13.4 | 0.41 | 0.86 | 50 | $2.0 \cdot e^4$ | $1.2 \cdot e^4$ | 1.636 ($\varphi$=40°) | 1.407 ($\varphi_{IL}$=35°) | 15 | |
| very dense | 13.4 | 0.21 | 1.00 | 50 | $6.5 \cdot e^4$ | $3.5 \cdot e^4$ | 1.636 ($\varphi$=40°) | 1.636 ($\varphi_{IL}$=40°) | $3 \cdot e^3$ | |

(*) $H_{s0}=6 \cdot e^3$, $\alpha_g=\alpha_f=0.45$, $\beta_0=4.2$, $\beta_1=0.2$, $\gamma=\gamma_u=2$

Note: $\gamma_s$ =solid grain density; e=void ratio; $D_r$=relative density, $\sigma'_{33}$=mean effective stress, $K_{ev0}$= bulk modulus, $G_0$= shear modulus, $M_g$= slope of critical state line in the q-p' space, $M_f$=slope of instability line in the q-p' space, $H_0$=hardening modulus

Parameters of the constitutive Pastor-Zienkiewicz (PZ) model used for simulating the experiments of Eckersley (1990).
207x69mm (300 x 300 DPI)

Table 2

| Case | $\gamma_{sat}$ (kN/m$^3$) | e (-) | $D_r$ (-) | $\sigma'_{33}$ (kPa) | $K_{ev0}$ (kPa) | $G_0$ (kPa) | $M_g$ (-) | $M_f$ (-) | $k_{sat}$ (m/s) | $H_0$(-) | (*) |
|---|---|---|---|---|---|---|---|---|---|---|---|
| dense (D) | 14.0 | 0.32 | 0.6 | 10 | $11.5 \cdot e^3$ | $25 \cdot e^3$ | 1.375 | 0.825 | $10^{-4}$ | 20 | |
| loose (L) | 14.0 | 0.62 | 0.4 | 10 | $11.5 \cdot e^3$ | $25 \cdot e^3$ | 1.375 | 0.550 | $10^{-4}$ | $1 \cdot e^{-2}$ | |

(*) $H_{u0}=6 \cdot e^3$, $\gamma=\gamma_u=2$, $\alpha_g=\alpha_f=0.45$, $\beta_0=4.2$, $\beta_1=0.2$

Note: $\gamma_{sat}$ =saturated soil unit weight; e=void ratio; $D_r$=relative density, $\sigma'_{33}$=mean effective stress, $K_{ev0}$= volumetric modulus, $G_0$= shear modulus, $M_c$= slope of critical state line in the q-p' space, $M_f$=slope of instability line in the q-p' space, $H_0$=hardening modulus

Mechanical behaviour of loose and dense soils used by Eckersley (1990): a) experimental evidence, b) numerical results, c) computed equivalent plastic strain versus ratio of mean effective stress to its initial value.
204x52mm (300 x 300 DPI)

Table 3

| Case | $\gamma_{sat}$ (kN/m$^3$) | e (-) | $D_r$ (-) | $\sigma'_{33}$ (kPa) | $K_{ev0}$ (kPa) | $G_0$ (kPa) | $M_g$ (-) | $M_f$ (-) | $k_{sat}$ (m/s) |
|---|---|---|---|---|---|---|---|---|---|
| 1 | 11.84 | 0.5 | 0.64 | 12.8 | $11.5 \cdot e^3$ | $25 \cdot e^3$ | 1.418 | 0.908 | $10^{-4}$ |
| 2 | 11.84 | 0.5 | 0.47 | 12.8 | $11.5 \cdot e^3$ | $25 \cdot e^3$ | 1.418 | 0.667 | $10^{-4}$ |

$H_0=H_{u0}=1 \cdot e^{-2}$, $\gamma=\gamma_u=2$, $\alpha_g=\alpha_f=0.15$, $\beta_0=1.2$, $\beta_1=0.2$

Note: $\gamma_{sat}$ =saturated soil unit weight; e=void ratio; $D_r$=relative density, $\sigma'_{33}$=mean effective stress, $K_{ev0}$= volumetric modulus, $G_0$= shear modulus, $M_g$= slope of critical state line in the q-p` space, $M_f$=slope of instability line in the q-p` space, $H_0$=hardening modulus

Soil mechanical parameters of slope shown in figure 9.
212x53mm (300 x 300 DPI)

# Modelling the post-failure stage of rainfall-induced landslides of the flow-type

Cascini L. (1), Cuomo S. (1), Pastor M. (2), Sacco C. (1)


## Abstract

The geomechanical modeling of failure and post-failure stages of rainfall-induced shallow landslides represents a fundamental issue to properly assess the failure conditions and recognize the potential for long travel distances of the failed soil masses.

Considering that these phenomena are among the most catastrophic natural hazard, as a contribution to the topic, the paper discusses the potentialities of a hydro-mechanical coupled FEM model to analyze the post-failure stage using an advanced constitutive model. Particularly, simple undrained triaxial tests and experimental evidences of centrifuge tests are reproduced firstly, for both cases of loose and dense soils. Then, two slope scale benchmarks are analyzed in the cases of vertical downward or horizontal water seepage and for both loose and dense soils. Compared with results obtained through standard limit equilibrium analyses, coupled FEM model provides a new comprehensive framework for failure and post-failure scenarios which includes a significant reduction of mean effective stresses also in the case of a loose soil slope subjected to vertical downward water seepage.

The obtained results are particularly encouraging since they outline the possibility to analyse in a unique framework both the failure and post-failure stages. Moreover, the numerical analyses indicate that the post-failure mechanisms are intimately tied to specific predisposing factors and boundary conditions, rather than to a single mechanical or state parameter of soil, such as for instance the soil relative density.


**Key words**: landslide; flow; failure; post-failure; acceleration; modelling


**(1) University of Salerno**
Lab. Geotechnics, Department of Civil Engineering
Via Ponte Don Melillo 1, 84084 Fisciano (SA), Italy

**(2) Universidad Politecnica de Madrid, Spain**
Department of Applied Mathematics and Computer Science
ETS Ingenieros de Caminos, UPM Madrid, Spain


**Definizione stile:** Stile 11 pt Giustificato Interlinea doppia: Rientro: Prima riga: 0.5 cm

**Formattato:** Stile 11 pt Giustificato Interlinea doppia, Allineato a sinistra, Interlinea singola, Controlla righe isolate

**Eliminato:** the

**Eliminato:** GeHoMadrid

**Eliminato:** GeHoMadrid

**Eliminato:** the

**Eliminato:** real

**Eliminato:** is

**Formattato:** Stile 11 pt Giustificato Interlinea doppia, Allineato a sinistra, Interlinea singola, Controlla righe isolate

**Formattato:** Stile 11 pt Giustificato Interlinea doppia, Allineato a sinistra, Interlinea singola, Controlla righe isolate

**Formattato:** Stile 11 pt Giustificato Interlinea doppia, Allineato a sinistra, Interlinea singola, Controlla righe isolate

## 1. Introduction

Landslides of the flow type still pose difficult challenges towards the combined geomechnical modelling of the failure and post-failure stages (Cascini et al., 2010) due to their mechanical characteristics. Particularly, the failure stage is characterized by the formation of a continuous shear surface through the entire soil mass (Leroueil, 2001) or, alternatively, plastic strains may affect a large amount of soil originating a so-called "diffuse" failure (Darve and Laoufa, 2000; Pastor et al., 2004); then, post-failure stage is represented by the rapid generation of large plastic strains and the consequent sudden acceleration of the failed soil mass (Hungr, 2004), often accompanied with a reduction of pore water pressures, which leads to a drastic increase of the landslide mobility. As a consequence, before failure onset, small soil deformations and displacements are measured (in coarse grained soils, soil deformations are even negligible) while at failure and during the post-failure stage, soil deformations rapidly increase up to some centimetres or metres. After that, the propagation stage occurs and displacements may attain values up to some kilometres, i.e. one or two orders of magnitude greater than the landslide source area dimension.

To date, valuable tools have been developed to model either failure (Leroueil, 2001; Pastor et al., 2007, Sanavia, 2009; among others) or propagation (McDougall & Hungr, 2004; Pastor et al., 2009; among others) and only few approaches (e.g. Pastor et al., 2002) refer to a unique mathematical framework to derive the governing equations which are then separately solved for analysing the triggering or propagation stage. The lack of a unified approach causes several difficulties and uncertainties in an appropriate hazard assessment related to a wide class of phenomena that can occur in both saturated and unsaturated conditions. To this regard, a good example is provided in figure 1 that shows a picture of two landslides occurred at Pizzo d'Alvano massif on May 1998 (Cascini et al., 2008); the first landslide (Fig. 1a) turned into a flow, later travelling about 1 km far; on the contrary, the second slide did not evolve into a landslide of the flow type and it was characterised by moderate displacements (Fig. 1b).

Considering the relevance of the topic, the present paper is aimed at proposing the use of new enhanced tools for geomechanical modelling. To this purpose, the available approaches for post-failure analysis are firstly discussed with some remarks proposed for both mechanical aspects and mathematical issues. Then, a hydro-mechanical coupled FEM model (Pastor et al., 1999, 2002) is shortly summarised and then proposed for modelling both the failure and post-failure stages within a unitary framework. Particularly, experimental

**Eliminato:** coupled

**Formattato:** Stile 11 pt Giustificato Interlinea doppia, Allineato a sinistra, Interlinea singola, Controlla righe isolate

**Eliminato:** and th

**Eliminato:** is

**Eliminato:** corresponds

**Eliminato:** ¶

**Eliminato:** furnished

**Eliminato:** ¶

**Eliminato:** filling the current gap, improving the current knowledge on the failure and post-failure stages also

**Eliminato:** approach

evidences derived from centrifuges tests are reproduced through a geomechanical modelling which is then extended to simple general slope schemes subjected to different water seepage conditions in both cases of loose and dense granular soils.

**Figure 1**

## 2. Literature review on post-failure stage

Post-failure stage is an outstanding topic since it discriminates different types of phenomena. In fact, it is quite evident that the chance for a landslide to achieve high velocities depends on: i) the initial acceleration of the failed mass and ii) subsequent transformation in a landslide of the flow type.

Anyway, the acceleration of the failed mass during the post-failure stage is associated to different mechanisms. Many Authors outline that the development of total or partial undrained conditions as the main cause of high pore-water pressures upon shearing. In particular, for loose unsaturated soils, volumetric collapse is discussed by Olivares & Damiano (2007), Yasufuku et al. (2005), Bilotta et al. (2006) and it is observed in constant-shear-drained triaxial tests upon wetting (Anderson and Riemer, 1995; Dai et al. 1999; Chu et al. 2003; Olivares & Damiano, 2007). For loose saturated soils, static liquefaction is introduced by Wang et al. (2002), Olivares & Damiano (2007), Van Asch et al. (2006) and observed in undrained triaxial tests (Lade 1992; Yamamuro and Lade 1998; Chu et al. 2003) as well as in undrained ring shear tests under controlled strain rates (Wang et al. 2002). Particularly, the build-up of pore pressures is shown to be relevant for soils having low density index (Eckersley 1990; Iverson 2000; Wang and Sassa 2001), fine grain size (Wang and Sassa 2003), low hydraulic conductivity (Iverson et al. 1997; Lourenco et al. 2006) and subjected to high deformation rate (Iverson et al. 1997).

The most of the above findings are obtained through laboratory tests such as isotropically consolidated undrained triaxial tests (ICU) (Chu et al., 2003), anisotropically consolidated undrained triaxial tests (ACU) (Eckersley, 1990), constant shear-drained triaxial tests (CSD) (Chu et al., 2003) even though strain localisation is more important under plane-strain or 3D conditions compared to triaxial conditions, as recently discussed by Wanatowski and Chu (2007, 2012). It is worth noting that all laboratory tests refer to idealized drainage conditions.

**Formattato:** Stile 11 pt Giustificato Interlinea doppia, Allineato a sinistra, Interlinea singola, Controlla righe isolate

**Formattato:** Stile 11 pt Giustificato Interlinea doppia, Allineato a sinistra, Interlinea singola, Controlla righe isolate

**Eliminato:** ¶

**Eliminato:** mostly

**Eliminato:** ,

**Eliminato:** et al.

**Eliminato:** which must refer to idealized drainage conditions.

On the other hand, a direct measurement of pressures and displacements in real slopes is rare, indeed only possible for: i) monitored sites during the occurrence of landslides, ii) artificially induced failure in real slopes. In both cases, measurements are not repeatable.

Further insights derive from alternative approaches which are based on direct observation of pore water pressures and stresses in landslides artificially induced in slope models at a reduced scale (also called flume test). Through this approach, information can be obtained on failure and post-failure (Eckersley, 1990); however, these experiments are expensive and since they reproduce the real processes at a greatly reduced scale they may be irrespective of the full-scale slope behaviour. For instance, a large difference in stress levels may exist between model and prototype; in particular, the eventual capillary suction is out of proportion with its self-weight stress, allowing the model slope to remain steeper than would be possible at higher effective stress levels. Nevertheless, complex groundwater conditions, such as downward rainfall infiltration from ground surface and/or a downwards/upwards water spring from the bedrock to the tested soil layer, can be analysed through these tests (Lourenco et al., 2006)

A more recent approach is based on centrifuge tests which reproduce stress levels similar to those experienced by a real slope. Centrifuge tests - except for some drawbacks such as the high costs and the availability of sophisticated equipments - combine the advantages of highly instrumented slopes (such as full/reduced scale models) with the potential of geometrical configurations realistically reproducing the in-situ conditions. Particularly, Take et al. (2004) point out that the transition from slide to flow is caused by local failures producing a variation in the slope geometry. This mechanism is related to transient localized pore-water pressures that are not associated to the development of undrained conditions, but originated by the combination of particular hydraulic boundary conditions and stratigraphical settings. Experimental evidences show that the transition from slide to flow can occur both for loose and dense soils and it can also correspond to decreasing pore-water pressures during the post-failure stage. These results have been later confirmed also by other researchers through small-scale flume tests (Lourenco et al. 2006) or centrifuge tests (Lee et al., 2008, Ng, 2009; among others).

Based on previous considerations, mathematical modelling may be outlined as a powerful tool because, in principle, it can be used to investigate a wide variety of different scenarios even though the modelling of the post-failure stage is poorly addressed in the literature and the only available contributions refer to triggering

Eliminato: 2007

Eliminato: well

Eliminato: et al.

Eliminato: ¶

factors that differ from rainfall, such as earthquake (Pastor et al. 2004) and kinematic or static perturbations (Laouafa and Darve 2002). For this reason, the basic concepts of the used approach are hereafter summarised and then applied to different benchmark cases to estimate the reliability of the numerical modelling to reproduce well know experimental results.

Eliminato: this

## 3. Proposed methodology

### 3.1 Conceptual reference scheme

Based on well established experimental evidences from laboratory and centrifuge tests, Cascini et al. (2010) propose a conceptual reference scheme to point out some key differences among different types of landslides during their failure and post-failure stages. Particularly, referring to different types of post-failure stages, Cascini et al. (2010) outline the existence of three main classes of phenomena: i.e. slide, flowslide, slide to flow. Slide is a slope failure occurring under pore water drained conditions. On the other hand, a flowslide occurs when partially or totally undrained conditions develop and this is the typical case of loose saturated soil upon shearing (i.e. static liquefaction); flowslides are associated to the increase of pore water pressures. Finally, the transition from a slide to a flow is caused by local failures producing a variation in the slope geometry which, in turn, determines an unbalanced driving force; this corresponds to a sudden increase of deviatoric stress at almost constant effective mean pressures.

Formattato: Stile 11 pt Giustificato Interlinea doppia, Allineato a sinistra, Interlinea singola, Controlla righe isolate

In the Authors' opinion, the features of the post-failure stage are strictly tied to the failure type and, in principle, the two stages should be analysed with a unitary approach. Moreover, the value attained by pore water pressures during the post-failure stage is a key issue for engineering purposes since it determines the soil mobility during the subsequent propagation stage. Therefore, some insights are hereafter proposed to individuate typical scenarios corresponding to the development of high pore water pressures in simple general slope schemes subjected to groundwater rainfall infiltration. It is important noting that a suitable approach should allow properly considering the twofold issue of Representative Elementary Volume (REV) and slope scale, particularly, i) the soil mechanical behaviour at REV scale, also including liquefaction phenomena and ii) at slope scale, the geometry constraints which predispose the failure and the hydraulic boundary conditions which determine the different triggering mechanisms.

Eliminato: s

### 3.2 Mathematical model

The adopted hydro-mechanical coupled model mainly derives from the fundamental contribution of Zienkiewicz at al. (1980, 1999) that considers a solid skeleton and two fluid phases, water and air, which fills the voids. The skeleton is made of particles of density $\rho_s$ with porosity $n$ (volume percent of voids in the mixture) and void ratio $e$ (volume of voids per unit volume of solid fraction). Movement of the fluid is considered as composed of two parts, the movement of soil skeleton and motion of the pore water relative to it. The total stress tensor acting on the mixture can be decomposed as the sum of an effective stress tensor σ' acting on soil skeleton and a hydrostatic pore pressure term $p_w$ which for unsaturated soils with zero air pressure corresponds to the averaged pore pressure $\bar{p} = S_r p_w$.

The governing equations of the model are reported in Cascini et al. (2010) and they consist in: i) balance of momentum equation for the mixture, ii) balance of mass of the pore water, iii) mass conservation for the pore fluid and iv) balance of momentum of the pore fluid. Those equations have to be complemented by a kinematic relation linking velocities to rate of deformation tensor, and a suitable constitutive model. The latter is the Pastor-Zienkiewicz (PZ) model which is suitable to accurately describe the behaviour of either loose or dense granular soils, both in drained and undrained conditions, along complex stress paths. In the PZ model, derived from the theoretical fundamentals of the Generalised Plasticity Theory (Pastor et al., 1990), it is assumed that plastic deformations may occur upon either loading or unloading and they are derived without the need to define the: i) yielding surface, ii) plastic potential surface, iii) consistency law. In details, the model is completely defined once the following quantities are fixed: i) three directions (load direction $n_{gL}$, unload direction $n_{gU}$ and neutral load direction n), ii) two scalars (plastic moduli $H_L$ and $H_U$) and iii) the elastic tensor $D_e$. Globally, 12 parameters are defined ($K_{ev0}$, $G_0$, $M_g$, $M_f$, $H_0$, $H_{u0}$, $\alpha_g$, $\alpha_f$, $\beta_1$, $\beta_0$, $\gamma$, $\gamma_u$); $K_{ev0}$ and $G_0$ are, respectively, the bulk modulus and shear modulus, $M_g$ and $M_f$ represent in the q-p' space the slope of critical state line and the slope of instability line (Chu et al., 2003), $H_0$ and $H_{u0}$ are hardening modulus in loading and unloading. Calibration of these parameters can be performed through standard triaxial tests according to the procedures indicated by Zienkiewicz et al. (1999) who also provide the values of some constants incorporated in the model, named $\alpha_g$, $\alpha_f$, $\beta_1$, $\beta_0$, $\gamma$ and $\gamma_u$. It is worth noting that $M_f$ is univocally related to the soil relative density as suggested by Pastor et al. (1990). The governing equations of







Eliminato: proposed paper
Eliminato: ¶
Formattato: Stile 11 pt Giustificato Interlinea doppia, Allineato a sinistra, Interlinea singola, Controlla righe isolate
Eliminato: ¶ ¶ T
Eliminato: soil constitutive
Eliminato: is
Eliminato: used since it
Eliminato: particularly
Eliminato: ¶
Eliminato:
Eliminato: and
Formattato: Pedice
Eliminato: $K_0$,
Eliminato: $\alpha_g$, $\alpha_f$,
Formattato: Tipo di carattere: 12 pt
Formattato: Tipo di carattere: 12 pt
Formattato: Tipo di carattere: 12 pt
Formattato: Tipo di carattere: 12 pt
Formattato: Tipo di carattere: 12 pt
Formattato: Tipo di carattere: 12 pt
Formattato: Pedice
Formattato: Tipo di carattere: 12 pt
Formattato: Tipo di carattere: 12 pt
Eliminato: , whose c
Formattato: Tipo di carattere: 12 pt
Eliminato: ion
Eliminato: Particularly,
Eliminato: the constitutive parameter
Eliminato: ,
Eliminato: which represents the slope of the instability line (Chu et al., 2003)

the hydro-mechanical coupled model are implemented in the FEM code named "GeHoMadrid FEM" whose details reported in Pastor et al. (1999, 2002).

Eliminato: ¶
¶

## 4. Testing the proposed approach

### 4.1. Benchmarks at REV scale

The hydro-mechanical response of a soil specimen during undrained triaxial tests is here simulated referring to the experiments of Eckersley (1990). The mechanical parameters are reported in Table 1 and they are calibrated referring to the procedure suggested by Zienkiewicz et al. (1999). Figure 2 shows the achieved results which match the experimental evidences; particularly, it can be reproduced either a strain-softening behaviour corresponding to the static liquefaction (very loose curve) or a strain-hardening soil response (very dense curve) which is typical of saturated dense sands upon undrained triaxial stress paths. The capability of the model to discriminate between the different behaviour of loose and dense soils is also outlined in figure 2c that shows the mean effective stress vanishing as the equivalent plastic strain ($\varepsilon_{eq}^{p} = (2/3 \cdot e^{p} : e^{p})^{1/2}$) increases in the case of "loose soil" while the opposite for "dense soil". The results of the simulated undrained triaxial tests are used as a reference case for discussion.

Eliminato: well

**Table 1**

**Figure 2**

### 4.2. Benchmarks from centrifuge tests

**Experimental evidence and Limit Equilibrium Analysis**

Moving from REV to slope scale, it is important to individuate simple general benchmarks to be referred with either standard or advanced approaches.

In the tests performed by Take et al. (2004), the slope configuration of figure 3a is used consisting in a layered shallow deposit 33° inclined over impervious bedrock. Due to permeability differences (coarser layer soils are more permeable than the upper ones), and imposed hydraulic boundary conditions (consisting in a water spring at the upper right corner of the model), transient groundwater seepage is observed in both layers and at the toe of the slope model.

Formattato: Stile 11 pt Giustificato Interlinea doppia, Allineato a sinistra, Nessuna, Interlinea singola, Controlla righe isolate

In the experiments, due to the increase of pore water pressures, a slope failure occurs and the sudden acceleration of the failed mass is measured for both cases of loose and dense soils (Fig. 3b). From the experimental evidences, it can be outlined the existence of different stages of the observed landslides. It is worth noting that the acceleration of the failed mass (i.e. post-failure stage) corresponds to the decrease of pore water pressures, mainly due to a concurrent modification of slope geometry (Fig. 3c).

**Figure 3**

To investigate the potential of standard tools, such as Limit Equilibrium Methods (LEMs), to adequately reproduce the above mentioned centrifuge tests, a proper set of scale relationships is taken into account between the centrifuge model (Fig. 3) and the equivalent prototype (Fig. 4a); scale relationships are related to the acceleration factor N used in the centrifuge tests. Consequently, the equivalent prototype is characterized by time and length scales multiplied by N while mechanical properties (eg. friction angle and permeability) and pressure/stress levels are equal to those acting during the tests. In their experiments Take et al. (2004) use a factor N equal to 30 and the equivalent prototype is shown in figure 4a and it reproduces the upper coarser soil layer of the centrifuge model. Take et al. (2004) also provide information on both groundwater conditions observed at failure onset and soil mechanical properties; the latter ones were also investigated through laboratory experiments described in GEO (1999) and Ng et al. (2004).

The limit equilibrium analyses are developed using the methods of Janbu (1954) and Morgenstern and Price (1965). The achieved results show that the slip surface with the minimum factor of safety individuates a soil volume which strictly corresponds to the highest values of the displacement field measured during the experiments (Fig. 4b). In conclusion, this simplified approach allows interpreting somehow the experimental results and it also outlines the severity of slope geometry and hydraulic boundary conditions which cause a strong reduction of the safety factor; however, it is not possible to provide any distinction between the case of loose and dense soil.

**Figure 4**

**Hydro-mechanical coupled stress-strain analyses**

**Formattato:** Stile 11 pt Giustificato Interlinea doppia, Allineato a sinistra, Interlinea singola, Controlla righe isolate

**Eliminato:** limit

**Eliminato:** e

**Eliminato:** m

**Eliminato:** S

**Eliminato:** as well as the groundwater condition observed at the failure are

**Eliminato:** available from the experiments of Take et al. (2004).

**Eliminato:** 1967

**Eliminato:** well approximates

The same centrifuge tests are here analysed using the proposed mathematical approach (sect. 3) and referring to the definitions of failure and post-failure given in section 1. In the numerical analyses an unstructured mesh is used with triangular elements on average not larger than 0.4 m. Adequate kinematic and hydraulic boundary conditions are selected to best reproduce the conditions imposed during the tests (Fig. 5). Particularly, a null pore water pressure values is assumed at point E - corresponding to the water table level observed at failure during the tests - to reproduce the raising of the water table in the upper soil layer. In the FEM analysis, pore water pressure is allowed to change in space and time, starting from an initial value of -5kPa throughout the slope model. This is adequately taken into account referring to Bishop's stresses (for details see Pastor et al., 2002, 2007). However, for sack of simplicity, numerical analyses are performed in the hypothesis of fully saturated conditions and the used version of the PZ constitutive model fits this hypothesis. Of course, the analyses could be extended to the case of unsaturated conditions but this is beyond the scope of the present paper.

The soil mechanical properties are reported in table 2 and they are either taken from GEO (1999), Ng et al. (2004) and Take et al. (2004), e.g. $\gamma_{sat}$, n, $M_g$ and $M_f$, or indirectly estimated/calibrated, e.g. $k_{sat}$, E, $\eta$, $H_0$, comparing the experimental evidences and the numerical results. It is worth noting that in table 2 different values of $M_f$ are assumed which derive from different values of relative soil density while the same critical friction angle ($M_g$) and bulk modulus ($K_{ev0}$) are considered for both loose and dense soils. This strong assumption is aimed at emphasizing in a limit case the role played by soil porosity as a fundamental factor for slope behaviour upon failure and beyond.

Hydro-mechanical coupled quasi-static analyses are performed to take into account the coupling between the solid skeleton and pore fluid. Numerical results and experimental evidences are compared referring to the following quantities: i) "equivalent centrifuge" times ($t_{centr}$), i.e. times relative to the prototype (numerical model) divided by the factor N, wich can be directly compared with those measured in centrifuge tests, ii) "centrifuge" displacements ($displ_{centr}$) computed in the same way, iii) pore water pressures and effective stresses as computed from the numerical modelling.

**Figure 5**

**Table 2**

**Formattato:** Stile 11 pt Giustificato Interlinea doppia, Allineato a sinistra, Interlinea singola, Controlla righe isolate

**Eliminato:** .

**Eliminato:** raising

**Eliminato:** For sake of simplicity, saturated soil conditions are assumed even if negative values of pore water pressures are also considered; furthermore, the initial pore water pressures are assumed equal to -5kPa throughout the slope model.

**Eliminato:** ¶

**Eliminato:** 1

**Eliminato:**

**Eliminato:**

**Eliminato:** an identical

**Eliminato:** i.e.

**Formattato:** Pedice

**Eliminato:** is

**Eliminato:** while different values of $M_f$ are assumed which derive from different values of relative soil density

**Eliminato:** ¶

**Eliminato:** ¶

**Formattato:** Didascalia;Didascalia Carattere1

Simulated plastic strains significantly differ in the case of loose and dense soil (Fig. 6) for both the value (larger for loose soil) and extent of the affected zone. In the case of loose soil, "diffuse" plastic strains are simulated, firstly at the toe of the slope (Fig. 6a), and then they involve a larger amount of the slope as time elapses. For dense soil (Fig. 6b), plastic strains appear firstly at the toe of the slope and then they are "localized" along a slip surface where plastic strains accumulate as the process evolves. The above mentioned differences depend only on the soil relative density values since all the other soil mechanical properties are assumed equal in the two cases. However, apart from the different type of failure, i.e. diffuse or localized, a different time evolution is also outlined (Fig. 7a). For loose soil, the failure stage is shorter because higher excess pore water pressures rapidly accumulate in the slope until it fails. Conversely, in the case of dense soil, both the pre-failure stage (mainly corresponding to elastic strains) and the failure stage are longer in time. These differences are also evidenced by the computed stress-paths and displacements in figure 7c and 7d. Globally, a slower slope response is observed for dense soil and this result completely agrees the experimental evidences of figure 3b. These results are further validated observing that in figure 3c pore water pressures are decreasing after failure in both cases; this process is reproduced in figure 7b.

Indeed, minor mismatches among the experimental and numerical results can be outlined: i) for dense soil, stiffer slope behaviour is outlined in the centrifuge test rather than in the numerical model (Fig. 3b and Fig 7d), ii) at failure, higher pore water pressures are simulated for dense soil rather than for loose soil. Regarding the former aspect, it must be noted that different stiffness values could be easily estimated and introduced in the numerical analyses for dense and loose soils (while they are assumed as equal); differently, the comparison of the obtained results for dense and loose soils could be confusing if not misleading. For the same reason, an equal soil conductivity is assumed for both cases of dense and loose soils; assuming a lower soil conductivity for dense soil, higher pore water pressure could be simulated. It is worth noting that the used model also correctly capture the onset of a yielding zone in the upper right corner, as shown by Lee et al. (2008).

As for the post-failure stage, it is of interest to note that, independently from the value of soil relative density, the failed mass accelerates (Fig. 7d), pore water pressure decrease as, respectively, evidenced by the experimental tests (Figures 3b and 3c).

**Figure 6**

**Formattato:** Non Evidenziato

**Formattato:** Stile 11 pt Giustificato Interlinea doppia, Allineato a sinistra, Interlinea singola, Controlla righe isolate

**Eliminato:** well defined

**Eliminato:** ¶
It is evident that the simulated plastic strains significantly differ in the case of loose and dense soil (Fig. 6) for both their absolute values (larger for loose soil) and the extent of the affected zone.

**Formattato:** Evidenziato

**Eliminato:** aspect

**Eliminato:** well

**Eliminato:** in both cases of figure 6,

**Eliminato:**

**Eliminato:**

**Eliminato:** .

**Figure 7**

## 5. New insights on post-failure stage

In order to evaluate the novelty and potentialities of the proposed approach compared to a uncoupled approach, two simple benchmarks at slope scale are hereafter analysed comparing the standard limit equilibrium analyses with hydro-mechanical coupled stress-strain analyses.

Particularly, the slope is composed of a homogeneous saturated soil being 10m high and 27° steep and it is subjected to two different quasi steady-state groundwater seepage conditions, i.e. sub-horizontal (case1) and vertical downwards directed (case 2), which are referred as limit cases of real seepage conditions in the final discussion. Soil mechanical properties are given in figure 8 and it is worth mentioning that a small cohesion (1kPa) is considered in all the numerical simulations to prevent local superficial failures which are not of interest in the paper being related to the steep slope geometry.

For case 1 (sub-horizontal seepage), the imposed hydraulic boundary conditions are: 1) an increasing water total head from 5 to 15 m at point A of figure 8, 2) a maximum pore water pressure equal to zero at slope surface, 3) pore water pressure equal to zero at boundary DE. Consequently, at the initial stage, a uniform field of nil pore water pressure is assumed, corresponding to a unity gradient seepage downwards; then, the water table is kept raising and the head isolines becoming somehow vertical and correspondingly the seepage velocities become quasi-horizontal. This leads to a general increase of pore water pressures in the whole slope up to failure onset.

For case 2 (sub-vertical seepage), the slope is subjected to a vertical groundwater seepage due to the following hydraulic boundary conditions: i) lateral boundaries impervious, ii) nil pore water pressures applied to the whole ground surface, iii) an imposed pore water pressures at the lower boundary (0 kPa at the initial stage, later increasing up to 20 kPa with a increment rate of $7e^{-3}$ kPa/s). Therefore, the infiltration velocities are always vertical; the hydraulic gradient is slowed down while pore water pressure values are increased in the slope due to the hydraulic boundary condition at the bottom of the slope.

**Figure 8**

### 5.1. Limit equilibrium analyses

Eliminato: an

Formattato: Stile 11 pt Giustificato Interlinea doppia, Allineato a sinistra, Interlinea singola, Controlla righe isolate

Formattato: Stile 11 pt Giustificato Interlinea doppia, Allineato a sinistra, Nessuna, Interlinea singola, Controlla righe isolate

Eliminato: :

Eliminato: ,

Eliminato: .

Formattato: Evidenziato

Eliminato: ¶

Formattato: Stile 11 pt Giustificato Interlinea doppia, Allineato a sinistra, Interlinea singola, Controlla righe isolate

Eliminato: ¶

Eliminato: ¶

Formattato: Stile 11 pt Giustificato Interlinea doppia, Allineato a sinistra, Interlinea singola, Controlla righe isolate

The results achieved through an uncoupled approach (Cascini et al., 2010) are based on a seepage analysis first and limit equilibrium analyses later. Pore water pressures are computed through the commercial code SEEP/W (Geoslope, 2005) and in figure 9 the isolines of total water head are shown at the final step of the analysis; pore water pressures are used as input data for limit equilibrium analyses performed through the methods of Morgenstern & Price (1965) and Janbu (1954) by using the SLOPE/W code (Geoslope, 2005). Several slip surfaces are considered with different shapes and depths and their safety factors are tracked with reference to the computed pore water pressures.

For case 1, due to a generalised increase of pore water pressures, factor of safety of the slope decreases in time from the initial value 1.65 up to 1. Particularly, the critical slip surface corresponds to the toe of the slope where high pore water pressures arise, thus drastically reducing the soil shear strength. For case 2, the initial value of safety factor is higher (1.8) and it decreases less than in the previous case up to the final value 1.6; failure is not predicted in this case.

In conclusion, the standard uncoupled limit equilibrium approach only outlines the importance of the groundwater regime for the attainment of limit equilibrium conditions in these two cases which are characterised by the same slope geometry.

**Figure 9**

### 5.2 Hydro-mechanical coupled stress-strain analyses

For both cases of figure 9, stress-strain analyses are performed referring to an unstructured mesh which is composed of 698 triangular elements, with 6 nodes each; the dimensions of the triangular elements are not larger than 2m and time steps of about 1s; the soil mechanical parameters of table 3 are used.

In the case of a sub-horizontal seepage condition (case 1), the results of stress-strain analysis outline that contours of the equivalent plastic strains and their value depend on soil density. For loose soil, plastic deformations concentrate along a slip surface, thus causing a triggering mechanism for a landslide (Fig. 10). For dense soil, plastic deformations only partially affect the toe of the slope while not causing a soil volume to be mobilized (Fig. 10). The different deformation modes affect the time evolution of the equivalent plastic strains (Fig. 10) and important differences can be observed when $p'/p_0$ (ratio of the mean effective pressure to its initial value) is plotted versus the equivalent plastic strain (Fig. 10). In fact, for loose soil, $p'/p_0$ reduces

Formattato: Stile 11 pt Giustificato Interlinea doppia, Allineato a sinistra, Interlinea singola, Controlla righe isolate

Eliminato: total

Eliminato: 1967

Formattato: Stile 11 pt Giustificato Interlinea doppia, Allineato a sinistra, Interlinea singola, Controlla righe isolate

Eliminato:

Eliminato:

Eliminato: ¶

Eliminato: ¶

up to 20% while a lower reduction is simulated in the case of dense soil; accordingly, failure is simulate for loose soils while not for dense soils.

Comparing these results with those of LEM analyses for case1, it comes out that both methods allow assessing the onset of failure. However, important differences are also outlined: i) FEM analyses provide a mobilized mass larger than LEM in the case of loose soils, ii) LEM is a conservative approach for the case of dense soil. It is convenient observing that the comparison of LEM and stress-strain FEM analyses is difficult to justify from a theoretical viewpoint, since LEM disregards non-associate flow rule and soil deformations. However, this comparison is meaningful for engineering purposes as both approaches provide the mobilized soil volume that can be quantitatively compared in the framework of engineering forecasting analyses. In addition, the comparison of LEM and FEM outlines the accuracy of LEM for different slope geometries and head water contours.

**Table 3**

**Figure 10**

Stress-strain analyses for the case of loose soil and sub-vertical groundwater seepage (case 2 of figure 9) show that pore water pressures increase due to the slope deformation; it is interesting noting that a large soil volume achieves high values of pore water pressures which cause the slope failure according to a diffuse mode (Fig. 11). Unlike the previous case of figure 8, pore water pressures undergo a generalised increase due to the soil response at REV scale; therefore, a large soil volume is involved in the slope failure. This generalised increase of pore water pressures does not require the effective mean stress p' to reach a very low value and failure is achieved when $p'/p_0$ reduces reach 60% (Fig. 11). Conversely, in the case of dense soils, failure is not simulated despite the same hydraulic boundary conditions have been applied (Fig. 11).

Comparing FEM and LEM results of case 2 and based on previous comments, it is not surprising to note that using LEM the safety factor is always higher than one (in both case of loose and dense soil) due to the drastic simplification made at REV scale in the LEM analysis. Conversely, coupled FEM analysis allows: i) accounting for a more realistic description of soil behaviour at REV scale and ii) adequately simulating the failure onset and post-failure stage that are both depending on soil density.

**Figure 11**

**Eliminato:** but
**Eliminato:** concern
**Eliminato:** coupled
**Formattato:** Inglese (Stati Uniti)
**Formattato:** Stile 11 pt Giustificato Interlinea doppia, Allineato a sinistra, Interlinea singola, Controlla righe isolate
**Eliminato:** 5
**Eliminato:** these
**Eliminato:** results with those of
**Eliminato:** analysis in
**Eliminato:** ; c
**Eliminato:** with
**Eliminato:** the
**Eliminato:** REV
**Eliminato:** is well modelled
**Formattato:** Evidenziato
**Eliminato:** it is possible to well simulate the onset of the
**Formattato:** Evidenziato
**Eliminato:** also the
**Eliminato:** which show different features
**Eliminato:** depending on
**Eliminato:** .

### 5.3 Discussion of the numerical results

An effort to provide some general results is here devoted to the analysis of pore water pressures variations during the failure and post-failure stages. Particularly, for all the above mentioned cases (soil REV, centrifuge tests and slope benchmarks), the achieved results are plotted with reference to two adimensional quantities: i) $\varepsilon_{pl}/\varepsilon_{pl}^{max}$, i.e. the ratio of equivalent plastic strains to its maximum value during the analysis and ii) $p'/p'_0$, the ratio of the mean effective stress to its initial value, later named normalized p' (Fig. 12). This variable $p'/p'_0$ has been formerly used by Pastor et al. (2007) for detecting via numerical modelling the occurrence of soil liquefaction due to earthquake and it is thought to be a useful factor to differentiate among distinct slope response to the applied hydraulic boundary conditions.

For the dense soil specimen the normalized p' decreases first and later increases, during the failure stage, accompanied with a very small strain rate; in such a case, this is the only failure mode compatible to the combination of soil mechanical features and imposed boundary conditions to stresses and pore pressures (i.e. undrained triaxial loading). In all the remaining cases, $p'/p'_0$ decreases while failure is approaching. Particularly, for the loose soil specimen a very low value of $p'/p'_0$ is reached because there isn't any possibility for the specimen to somehow react against the imposed boundary conditions. Different patterns are drawn for centrifuge tests which, at point P of figure 5, exhibit first a drastic reduction of $p'/p'_0$ (failure stage) due to the severe slope geometry and then a moderate increase of $p'/p'_0$ (during the post-failure stage) mainly due to a change of slope geometry and consequent increase pore water pressure; this behaviour is more exacerbated for loose than dense soils. Whereas, a gradual reduction of $p'/p'_0$ is modelled at point P of figure 8, for the case of quasi-horizontal seepage with the lowest value reached for loose soil. Finally, for the case of quasi-vertical seepage, a different slope behaviour is simulated with a reduction of $p'/p'_0$ for loose soils but not for dense soils. In conclusion, an important mutual interplay among soil REV response, stress conditions (plane-strain or axial symmetric), slope geometry and hydraulic

Formattato: Stile 11 pt Giustificato Interlinea doppia, Allineato a sinistra, Interlinea singola, Controlla righe isolate

Formattato: Rientro: Prima riga: 0.5 cm

Eliminato: factor

Eliminato: ¶

Eliminato: Firstly, it can be observed that $p'/p_0$

Eliminato: is in

Eliminato: ing

Eliminato: only for dense soil specimen

Eliminato: this

Eliminato: possible

Eliminato: for failure to occur due

Eliminato: to the

Eliminato: and

Eliminato: is

Eliminato: ing

Eliminato: at

Eliminato: certain

boundary conditions is shown; this interplay really determines the global slope behaviour.

**Figure 12**

## 6. Concluding remarks

The application of the proposed methodology to both centrifuge evidences and two simple benchmarks highlights some general insights. Particularly, it is shown that the slope response is controlled by two different "driving mechanisms": i) the generation of excess pore water pressures, and ii) localization of plastic strains. The former mechanism is typical of loose saturated sands and it controls the soil behaviour at REV scale; in fact, for loose soils, high pore water pressures are simulated also due to soil deformation. The latter mechanism is typical of dense soils and it is acting at slope scale; in this sense, the chance for localised strains to develop depend on: i) slope geometry (steep slope), ii) stress conditions (plain-strain rather than triaxial) and iii) local boundary conditions (groundwater impoundments) that enhance the local generation of high plastic strains and the subsequent development of a slip surface.

Based on the achieved results it is outlined that: i) in the practical applications the case of loose soils must be surely taken into account for the possible failure and post-failure stage scenarios, ii) the case of dense soils also deserves a special attention because, depending on slope geometry and boundary conditions, it may correspond to scenarios of brittle localised failures which imply a sudden acceleration of the failed mass which cause a slide to turn into a flow.

**Acknowledgements**

The authors would like to dedicate this paper to the memory of the recently departed Prof. Giuseppe Sorbino. His vitality, optimistic nature, and many other human and scientific qualities will be very much missed.

**Figure captions**

**Figure 1.** Examples of landslides occurred at Pizzo d'Alvano massif on May 1998: a) slides evolved into a landslide of the flow type; b) in the same are, an example of slide not evolved into a flow.

Formattato: Stile 11 pt Giustificato Interlinea doppia, Allineato a sinistra, Interlinea singola, Controlla righe isolate

Eliminato: I

Eliminato: was

Eliminato: localization

Eliminato: driving

Eliminato: driving

Eliminato: may

Eliminato: As a consequence of

Eliminato: can be stated

Formattato: Stile 11 pt Giustificato Interlinea doppia, Allineato a sinistra, Interlinea singola, Controlla righe isolate

**Table 1.** Parameters of the constitutive Pastor-Zienkiewicz (PZ) model used for simulating the experiments of Eckersley (1990).

**Figure 2.** Mechanical behaviour of loose and dense soils used by Eckersley (1990): a) experimental evidence, b) numerical results, c) computed equivalent plastic strain versus ratio of mean effective stress to its initial value.

**Figure 3.** Observed behaviour of centrifuge slope model for loose and dense soils: a) centrifuge model, b) displacement measured at PIV1, c) pore water pressures measured at PPTT1 (modified from Take et al., 2004).

**Figure 4.** a) Results of limit equilibrium analysis, b) comparison between the computed critical slip surface and the experimental evidence from Take et al. (2004).

**Figure 5.** Slope scheme used for the numerical analyses.

**Table 2.** Soil mechanical parameters for simulation of centrifuge test

**Figure 6.** Time evolution of equivalent plastic strains computed for loose and dense soil (case "L" and "D" of table 2).

**Figure 7.** Results for the node P of figure 5: a) equivalent plastic strains, b) pore water pressures, c) stress path in the p'-q plane, d) horizontal displacements versus time.

**Figure 8.** New slope benchmarks to test the proposed approach.

**Figure 9.** Results of limit equilibrium analyses for slope benchmarks.

**Table 3.** Soil mechanical parameters of slope shown in figure 9

**Figure 10.** Results of numerical analyses for the case of sub-horizontal seepage (case 1).

**Figure 11.** Results of numerical analyses for the case of sub-vertical seepage (case 2).

**Figure 12.** Ratio of equivalent plastic strain to its maximum value (x-axis) versus the ratio of mean effective pressure to its initial value (y-axis) for different analysed cases.

## 7. References

1. Anderson, S.A and Riemer. M.F., 1995. Collapse of saturated soil due to reduction in confinement. Journal of Geotechincal Engineering ASCE 121 2, 216-220.
2. Bilotta, E., Foresta, V. and Migliaro, G. 2006. Suction controlled laboratory tests on undisturbed

**Eliminato:** the Pastor-Zienkiewicz (PZ) model

**Eliminato:** for the Pastor-Zienkiewicz (PZ) model.

**Formattato:** Stile 11 pt Giustificato Interlinea doppia, Allineato a sinistra, Interlinea singola, Controlla righe isolate

pyroclastic soil: stiffnesses and volumetric deformations. Proc. International Conference on Unsaturated Soils, 2-6 April, Carefree, Arizona USA, 1, 849-860

3. Cascini, L., Cuomo, S. and Guida, D. 2008. Typical source areas of May 1998 flow-like mass movements in the Campania region, Southern Italy. Engineering Geology, 96, 107-125.

Cascini, L., Cuomo, S., Pastor, M. and Sorbino, G. 2010. Modelling of rainfall-induced shallow landslides of the flow-type. ASCE's Journal of Geotechnical and Geoenvironmental Engineering, 1, 85-98.

Chu, J., Leroueil, S., and Leong, W. K. 2003. Unstable behaviour of sand and its implications for slope instability. Canadian Geotechnical Journal, 40, 873-885.

4. Dai, F., Lee, C.F., Wang, S. and Feng Y. 1999. Stress-strain behaviour of a loosely compacted volcanic-derived soil and its significance to rainfall-induced fill slope failures. Engineering Geology, 53, 359-370.

5. Darve, F. and Laouafa F. 2000. Instabilities in granular materials and application to landslides. Mechanics of Cohesive frictional Materials, 58, 627-652.

6. Eckersley D. 1990. Instrumented laboratory flowslides. Géotechnique, 40, 489-502.

7. Geotechnical Engineering Office (1999) Slope No. 11NW-B/FR61, Beacon Hill Radar Airport Station, Final Laboratory Testing Report, Geotechnical Engineering Office, Civil Engineering Department, The Government of the HKSAR.

8. Geoslope 2005. User's guide. GeoStudio 2004, Version 6.13. Geo-Slope Int. Ltd. Calgary, Canada.

9. Hungr, O. 2004. Flow slides and flows in granular soils. Proc. of the Int. Workshop Flows 2003 - Occurrence and Mechanisms of Flows in Natural Slopes and Earthfill, Sorrento, Patron Ed..

10. Iverson 2000. Landslide triggering by rain infiltration. *Water Resources Research*, 367, 1897-1910.

11. Iverson, R.M., Reid, M.E. and LaHusen R.G. 1997. Debris flow mobilization from landslides. Annual Review Earth Planet. Science, 25, 85-138.

12. Janbu, N. 1954. Application of Composite Slip Surface for Stability Analysis. European Conference on Stability Analysis, Stockholm, Sweden.

13. Lade, P.V. 1992. Static instability and liquefaction of loose fine sandy slopes. Journal of Geotechnical Engineering ASCE, 118 1, 51-71.

14. Laouafa, F. and Darve F. 2002. Modelling of slope failure by a material instability mechanism.

**Formattato:** Stile 11 pt Giustificato Interlinea doppia, Allineato a sinistra, Interlinea singola, Nessun elenco puntato o numerato, Controlla righe isolate

Computers and Geotechnics, 29, 301-325.

15. Lee, Y.S., Cheuk, C.Y., and Bolton, M.D. (2008) Instability caused by a seepage impediment in layered fill slopes. Canadian Geotechnical Journal, 45(10), 1410-1425.
16. Leroueil S. 2001. Natural slopes and cuts: movement and failure mechanisms. Geotechnique, 51, 3, 197-243.
17. Lourenco, S., Sassa, K. and Fukuoka, H. 2006. Failure process and hydrologic response of a two layer physical model: Implications for rainfall-induced landslides. Geomorphology, 731-2, 115-130.
18. McDougall, S., Hungr, O., 2004. A model for the analysis of rapid landslide motion across three-dimensional terrain. Canadian Geotechnical Journal, 41, 1084-1097.
19. Morgenstern, N.R. and Price, V.E. 1965. The analysis of the stability of general slip surfaces. Geotechnique, 151, 79-93.
20. Ng CWW, Fung WT, Cheuk CY, Zhang L (2004) Influence of stress ratio and stress path on behaviour of loose decomposed granite. ASCE Journal of Geotechnical and Geoenvironmental Engineering 130(1): 36-44.
21. Ng, C.W.W. 2009. What is Static Liquefaction Failure of Loose Fill Slopes? In: The first Italian Workshop on Landslides Napoli 8-10 giugno 2009 NAPOLI Doppiavoce. Studio editoriale Vol.1, pp. 43-51 ISBN:9788889972120
22. Olivares, L. and Damiano, E. 2007. Postfailure Mechanics of Landslides: Laboratory Investigation of Flowslides in Pyroclastic Soils. Journal of Geotechnical and Geoenvironmental Engineering ASCE, 1331, 51-62.
23. Pastor M., Fernández Merodo J.A., Herreros M.I., Mira P., González E., Haddad B., Quecedo M., Tonni L. Drempetic V. 2007. Mathematical,Constitutive and Numerical Modelling of Catastrophic Landslides and Related Phenomena. Rock Mechanics and Rock Engineering, 411, 85-132
24. Pastor, M., Fernandez-Merodo, J.A., Gonzalez, E., Mira, P., Li, T. and Liu, X. 2004. Modelling of landslides: I. Failure mechanisms. Degradations and Instabilities in Geomaterials, CISM Course and Lectures No. 461, Darve F. and Vardoulakis I. ed., Springer-Verlag, 287-317.
25. Pastor, M., Haddad, B., Sorbino, G., Cuomo, S. and Drempetic, V. 2009. A depth-integrated, coupled SPH model for flow-like landslides and related phenomena. Int. J. Numer. Anal. Meth. Geomech 33:

**Formattato:** Rientro corpo del testo 2, Giustificato, Rientro: Sinistro: 0.12 cm, Numerazione automatica + Livello:1 + Stile numerazione: 1, 2, 3, … + Comincia da:1 + Allineamento: A sinistra + Allinea a: 1.14 cm + Rientra di: 1.77 cm, Nessun controllo righe isolate

**Eliminato:** ¶

**Formattato:** Giustificato

**Eliminato:** &

143-172.

26. Pastor, M., Li, T., Liu, X. and Zienkiewicz, O.C. 1999. Stabilized low order finite elements for failure and localization problems in undrained soils and foundations. Comput. Methods Appl. Mech. Engrg. 174, 219-234.
27. Pastor, M., Quecedo, M., Fernandez-Merodo, J.A., Herreros, M.I., Gonzalez, E. and Mira P. 2002. Modelling tailing dams and mine waste dumps failures. Geotechnique, 528, 579-591.
28. Pastor, M., Zienkiewicz, O.C. and Chan, A.H.C. 1990. Generalized plasticity and the modelling of soil behaviour. Int. J. Numer. and Anal. Methods in Geomechanics, 14, 151-190.
29. Sanavia, L. 2009. Numerical modelling of a slope stability test by means of porous media mechanics. Engineering Computations (Swansea, Wales) 26 (3), 245-266.
30. Take, W.A., Bolton, M.D., Wong, P.C.P. and Yeung F.J. 2004. Evaluation of landslide triggering mechanisms in model fill slopes. Landslides, 1, 173-184.
31. Van Asch, Th.W.J. , Malet, J.P. and van Beek L.P.H. 2006. Influence of landslide geometry and kinematic deformation to describe the liquefaction of landslides: Some theoretical considerations. Engineering Geology, 88, 59-69.
32. Wang, F.W., Sassa, K. and Wang G. 2002. Mechanism of a long-runout landslide triggered by the August 1998 heavy rainfall in Fukushima Prefecture, Japan. Engineering Geology, 63, 169-185.
33. Wang, G. and Sassa K. 2001. Factors affecting rainfall induced landslides in laboratory flume tests. Géotechnique, 51, 587-600.
34. Wang, G. and Sassa, K. 2003. Pore-pressure generation and movement of rainfall-induced landslides: effects of grain size and fine-particle content. Engineering Geology, 69, 109-125.
35. Yamamuro, J.A. and Lade P.J. 1998. Steady-state concepts and static liquefaction of silty sands. ASCE J Geotech Geoenviron Eng, 1249, 868-878.
36. Yasufuku, N., Ochiai, H. and Hormdee, D. 2005. An empirical relationship for evaluating collapsible settlements of volcanic ash sandy soil. Advanced experimental unsaturated soil mechanics. Tarantino, Romero and Cui ed., 265-272.
37. Zienkiewicz, O.C., Chan, A.H.C., Pastor, M., Shrefler, B.A. and Shiomi T. 1999. Computational Geomechanics. J.Wiley and Sons.

Formattato: Giustificato

Eliminato: &

686 38. Zienkiewicz, O.C., Chang C.T. and Bettess P. 1980. Drained, undrained, consolidating dynamic
687 behaviour assumptions in soils. Geotechnique, 30, 385-395.